Cross-Bridge Elasticity in Single Smooth Muscle Cells

DAVID M. WARSHAW and FREDRIC S. FAY

From the Department of Physiology, University of Massachusetts Medical School, Worcester, Massachusetts 01605

ABSTRACT In smooth muscle, a cross-bridge mechanism is believed to be responsible for active force generation and fiber shortening. In the present studies, the viscoelastic and kinetic properties of the cross-bridge were probed by eliciting tension transients in response to small, rapid, step length changes (ΔL = 0.3–1.0% L_{cell} in 2 ms). Tension transients were obtained in a single smooth muscle cell isolated from the toad (*Bufo marinus*) stomach muscularis, which was tied between a force transducer and a displacement device. To record the transients, which were of extremely small magnitude (0.1 μN), a high-frequency (400 Hz), ultrasensitive force transducer (18 mV/μN) was designed and built. The transients obtained during maximal force generation (F_{max} = 2.26 μN) were characterized by a linear elastic response (E_{max} = 1.26 × 10^4 mN/mm^2) coincident with the length step, which was followed by a biphasic tension recovery made up of two exponentials (τ_{fast} = 5–20 ms, τ_{slow} = 50–300 ms). During the development of force upon activation, transients were elicited. The relationship between stiffness and force was linear, which suggests that the transients originate within the cross-bridge and reflect the cross-bridge's viscoelastic and kinetic properties. The observed fiber elasticity suggests that the smooth muscle cross-bridge is considerably more compliant than in fast striated muscle. A thermodynamic model is presented that allows for an analysis of the factors contributing to the increased compliance of the smooth muscle cross-bridge.

INTRODUCTION

The cyclic interaction of myosin cross-bridges with actin filaments in smooth muscle is believed to be responsible for force production and active cell shortening (Murphy, 1976; Fay et al., 1981). Although this contractile mechanism is purportedly similar to that in striated muscle, several aspects of its contraction are quite different. The maximum velocities of shortening and the actomyosin ATPase are much slower in smooth as compared with striated muscle. In addition, smooth muscle

Address reprint requests to Dr. David M. Warshaw, Dept. of Physiology, University of Massachusetts Medical Center, 55 Lake Ave. North, Worcester, MA 01605.

J. GEN. PHYSIOL. © The Rockefeller University Press · 0022-1295/83/08/0157/43 $1.00 157
Volume 82 August 1983 157–199

maximum force production normalized to muscle cross-sectional area is comparable to, if not greater than, in striated muscle, however, requiring much less myosin. Although the difference in smooth muscle's physiological properties relative to striated muscle might reflect the manner in which cells are interconnected within the tissue, it is now agreed that these distinguishing characteristics are in fact an inherent property of the individual cells. Therefore, differences must exist within the basic contractile mechanism in order to account for these unique physiological characteristics. These differences may in fact reside within the cross-bridge, whose mechanics and/or kinetics of interaction with actin may be altered.

The cross-bridge cycle is envisioned as a multistep process having both attached and detached cross-bridge states that are involved in the production of force and fiber shortening. In 1923, Fenn observed that the rate of heat production in muscle was highly dependent upon the velocity of shortening (Fenn, 1923). This observation was of major importance, because it suggested that the rate of the actomyosin ATPase is determined by the physical constraints placed upon the muscle. It is believed that the variation in the rate of actomyosin ATPase with muscle shortening reflects the sensitivity of several steps within the cycle to the cross-bridge position relative to its actin binding site. Therefore, investigators have employed various length (Huxley and Simmons, 1971) and force (Podolsky and Nolan, 1972) perturbations as a means of probing the transitions between cross-bridge states (i.e., cross-bridge kinetics). Specifically, when small rapid step changes in length were applied to single frog striated muscle fibers, the resulting multiphasic tension transients were interpreted as reflecting the mechanical response of the cross-bridge (phase 1; cross-bridge elasticity), followed by the transitions of a relatively synchronized population of cross-bridges as they pass through a series of steps in the cycle involved in force production (Ford et al., 1977). Although similar studies on whole smooth muscle have not revealed transients similar to those observed in striated muscle (Halpern et al., 1978; Hellstrand and Johansson, 1979; Mulvany, 1979; Pfitzer et al., 1982), this may reflect heterogeneity in the response of a multicellular preparation, thereby masking the response of the individual cells. To avoid the complexities inherent in a multicellular preparation, we have developed techniques required to record tension transients from single isolated smooth muscle cells (SMC) in response to small rapid length steps during isometric force production.

In contrast to studies on intact tissues, the tension transients from single SMC suggest that they originate within the cross-bridge and that cross-bridge elasticity may be linear in smooth as in striated muscle. In addition, the rates of tension recovery are faster than those previously reported for smooth muscle. This paper will be the first in a series dealing with the mechanics as well as the kinetics of the cross-bridge cycle in single SMC. This paper will present the techniques that were required to record tension transients from a single SMC. The analysis of the tension tran-

sients, however, will be divided into two parts. The first part described in this paper will deal in detail with the elastic properties of the cell and will address the origin of this elastic response. The second paper will address the kinetics of the cross-bridge cycle in SMC by analyzing the time course of tension recovery in response to a length step. Finally, the last paper in this series will attempt to incorporate the tension transient data into a detailed thermodynamic model of the cross-bridge cycle, and to relate cross-bridge cycle parameters to the unique physiological characteristics of smooth muscle contraction.

METHODS

System Description

An overview of the techniques and instrumentation required to record force from a single SMC will be presented here. In subsequent sections, we will describe in detail the isolation and preparation of SMC as well as the design and construction of the instrumentation needed to perform the present series of experiments.

SMC were isolated by enzymatic digestion of the stomach muscularis of the toad, *Bufo marinus.* An aliquot of cells (0.1 ml at 10^6 cells/ml) was transferred to a glass slide containing 10 ml of amphibian physiological saline (APS) with 10^{-6} M isoproterenol as a relaxing agent. The slide was then placed upon the stage of an inverted microscope (Carl Zeiss, Inc., Thornwood, NY), and the cells were allowed to settle. The cell was then firmly attached with a micromanipulator and special microprobes to a force transducer and a piezoelectric length displacement device whose motion was detected by an eddy current displacement sensor (Figs. 1 and 2). Both the force and length signals were recorded simultaneously on FM tape and a chart recorder. The tape-recorded data were digitized at 2.5 kHz and stored on computer storage discs for later analysis. The image of the cell was magnified ×400 under bright field illumination. Using a beam splitter, direct observations of the cell were possible as well as continuous video monitoring and recording (Sony Corp. of America, Long Island City, NY). At the same time, a second video camera focusing on the chart recorder allowed the chart image to be monitored on a split screen with the image of the cell so that correlation of gross cell length and force traces was possible. Cells were stimulated to contract by electrical field stimulation using two platinum paddles (surface area = 0.43 mm^2) that straddled the entire length of the cell. Square-wave 70-V DC pulses of 0.1 ms duration were routinely used to maximally contract these cells.

CELL PREPARATION Although a detailed description of the method for isolation of single SMC has recently been reported (Fay et al., 1982), a brief description is included here. Toads were killed by decapitation, the stomach was excised, and mucosa was dissected away. The remaining muscularis and serosal layers were cut into fine slices (0.5 mm thick, 5 mm square) and then incubated in APS containing both trypsin and collagenase at 30°C for 45 min with constant gentle agitation. The tissue was then removed and rinsed with bovine serum albumin in APS and finally incubated in APS containing collagenase for 30–90 min to obtain maximal cell density. The cells remained viable for 24 h when placed in an APS solution containing soybean trypsin inhibitor and gentamycin.

CELL KNOTTING AND MICROPROBE CONSTRUCTION To facilitate manipulation and attachment of SMC to both the force transducer and the displacement device, special microprobes were constructed in the following manner. Glass

tubing (0.81 mm OD, 0.56 mm ID) was drawn to a fine tip (0.25–0.50 μm diam). The rods were then cut to either 25 mm to be used on the piezoelectric displacement device or 5 mm for the force transducer. A glass slide having a thin layer of fresh silicone rubber cement (Dow Corning Corp., Midland, MI)

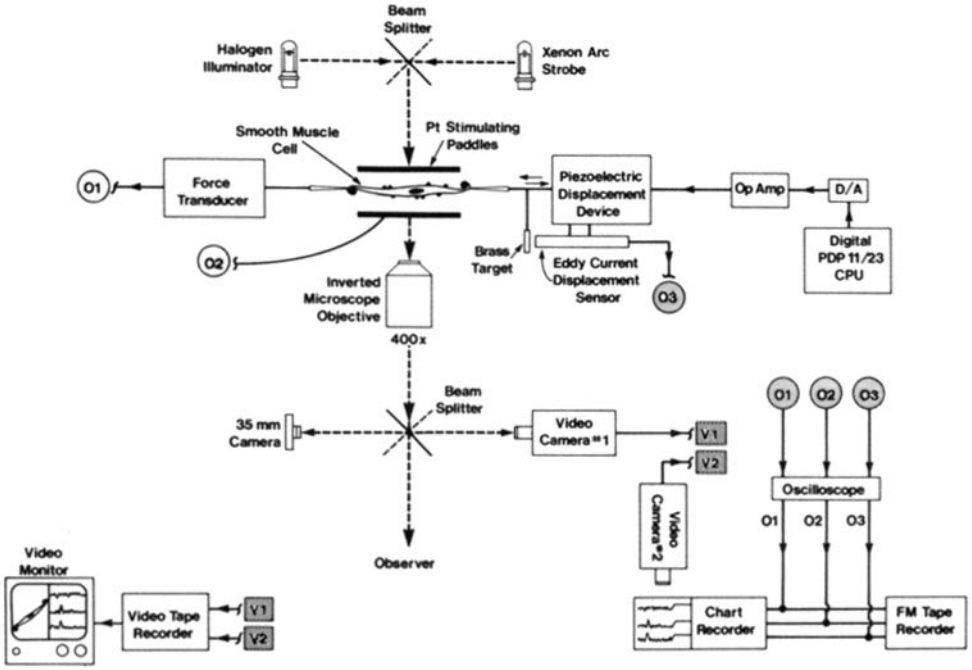

FIGURE 1. Instrumentation block diagram. A single SMC was attached as described in text to a force transducer (FT) and piezoelectric displacement device (PDD) capable of imposing small step length changes. The output of the FT (01) and an eddy current displacement sensor (03) that detected the motion of a brass target attached to the PDD were monitored on oscilloscopes as was the stimulating pulse (02) that initiated contraction. These signals (01, 02, 03) were stored on FM tape and recorded by a chart recorder. The length steps were controlled and generated by computer (PDP 11/23). The length step signal had to be amplified by a high-voltage operational amplifier (Op Amp) before it entered the PDD. Throughout the experiment, the cell's image could be observed at ×400 through an inverted microscope. This image was recorded on video tape (V1) simultaneously with the image of the chart record (V2). Both images were viewed on a split-screen video monitor. Recording of double-exposure flash photographs was accomplished by rotating the beam splitter to allow the xenon arc strobe flash to expose film in a 35-mm camera.

was placed on the microscope stage. The very end of the pipette tip was dipped into and out of the cement with a micromanipulator. The slide with cement was then removed and replaced with a slide having a smear of anionic exchange resin beads (Aminex; Bio-Rad Laboratories, Richmond, CA; 20 μm diam). The glue-covered tip was then brought into contact with a single bead, which adhered to

it. The microprobe with a bead glued to its end was then stored in a microelectrode jar (W-P Instruments, Inc., New Haven, CT) and the cement was allowed to cure. After curing and before use, the microprobe was dipped first in 1 N NaOH and then in 1 N HCl, giving the bead its positive charge. The microprobes were then attached to the force transducer and piezoelectric translator using beeswax (Aloe Scientific).

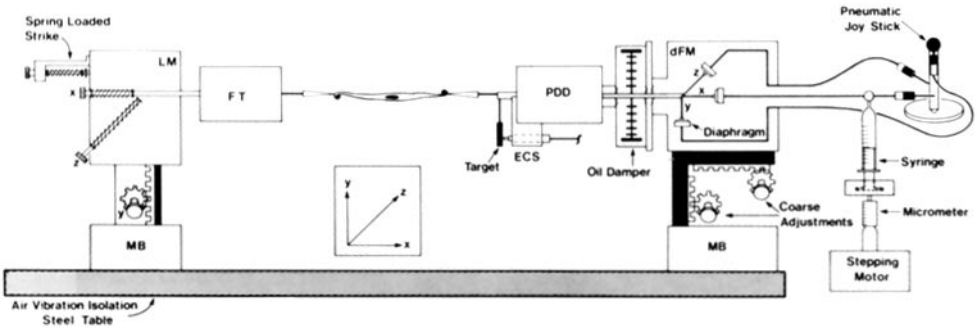

FIGURE 2. Mechanical diagram. To facilitate manipulation of a single SMC for recording tension transients in response to step length changes, the mechanical system was arranged as follows. The force transducer (FT) and piezoelectric displacement device (PDD) were mounted on Leitz (LM) and de Fondbrune (dFM) micromanipulators, respectively. Both micromanipulators were mounted on magnetic bases (MB) to secure the LM and dFM to the air suspension steel vibration isolation table. Gross positioning of the FT and PDD was accomplished by course adjustments in the *X*, *Y*, and *Z* axes. Fine micromanipulation necessary for tying the cell was performed using a joystick that controlled the pneumatic diaphragms of the dFM, which in turn determined the microprobe position that was attached to the PDD. Mechanical vibrations within the dFM diaphragms initiated by the rapid motion of the PDD were eliminated by designing an oil damper placed between the PDD and dFM. In addition to small length steps generated by the PDD, longer length steps (50 μm) were obtained using a 50-ml syringe as an auxillary air bellows in line with the *X*-axis dFM diaphragm. Volume changes in the syringe were initiated by a stepping motor/micrometer drive that moved the syringe plunger. To determine the FT mechanical properties, a spring-loaded striker attached to the LM was drawn back a fixed amount and released, effecting an impulse input to the FT.

With the use of a micromanipulator, a microprobe with a positively charged bead was brought into contact with one end of a single cell. The cell would electrostatically attach to the bead and via this attachment the cell could be freely maneuvered within the solution. A second microprobe was then brought into contact with the other end of the cell for a similar electrostatic attachment. The knotting procedure would then begin (Fig. 3). All maneuvers were performed with the micromanipulator that controlled the microprobe attached to the length translator (Fig. 2) because the position of the force transducer microprobe remained fixed. Two double Blackwall's hitches (The Sea Scout Manual, 1939)

using approximately one-third of the cell were tied at both ends as seen in Fig. 3. Once the loose knots had been tied, the cell was stretched taut by imposing slow (i.e., 1 s) 10-μm length changes at 20-s intervals to avoid sudden activation

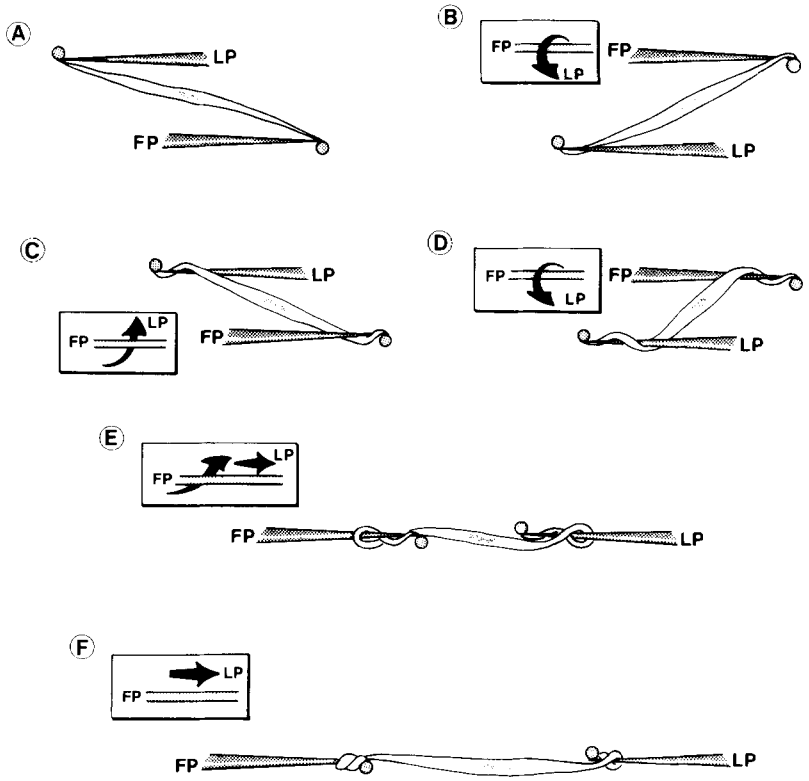

FIGURE 3. Procedure for tying a single smooth muscle cell to microprobes. A single cell was first attached electrostatically, as in *A*, to anionic exchange resin beads at the end of microprobes attached to a force transducer (FP) and length displacement device (LP). To secure the cell firmly to the microprobes, a knot (Blackwall's Hitch) was tied (see text). The cell was wrapped around each microprobe using the joystick control on the de Fondbrune micromanipulator (see Fig. 2) by first bringing LP underneath FP and to the opposite side of FP (*B*). Then LP was returned to its starting position as in *B* by bringing LP over FP (*C*). Step *B* was repeated, resulting in *D*. To obtain the cell overlap needed to fasten the knots, LP was brought over and out along the cell's long axis (*E*). To finally secure the knot, the cell was slowly stretched until the knots were tight and 0.2 μN of passive force was recorded in response to a 10-μm stretch. Although only one knot is illustrated, this procedure is continued until several knots have been obtained.

of the cell. Knots were considered tight when in response to a slow 10-μm stretch, 0.2 μN of passive tension was recorded and when no further motion of the cell in the knotted region could be observed. After the knotting procedure, approx-

imately two-thirds of the cell length remained between the probes. It was at this point that the mechanical experiments would begin.

Force Transducer

An ultrasensitive force transducer capable of measuring minute forces in the micronewton range that were characteristically produced by a single SMC was designed and more recently improved in our laboratory. The improvements were required so that tension transients resulting from small, rapid length changes could be accurately measured with a frequency response of 400 Hz. A detailed description of an earlier version is available (Canaday and Fay, 1976); therefore, only a brief description of the force transducer and its most recent improvements will be included here.

The force transducer (Fig. 4*A*) is a photo-optical system that relates the amount of light transmitted through a pair of Ronchi-ruled gratings to the SMC's force production. The SMC is attached by means of a microprobe (as discussed earlier) to the transducer's moving element (Fig. 4*B*). As the SMC contracts, it tugs (*X* axis, see Fig. 4*A* and *B*) on the moving element, thereby displacing the moveable grating past a fixed grating. The displacement of the gratings relative to each other results in a change in the transmitted light intensity.

The moving element is constructed of two glass support beams and a cross-member to which a circular, glass (3 mm diam, Corning 00; Corning Glass Works, Corning, NY), photoetched replica of a Ronchi-ruled grating (250 lines/in.; Gauge Line Sciences, Rochester, NY) is affixed by epoxy (5-min epoxy; Devco Engineering Inc., Fairfield, NJ). The joints between the support beams and cross-member are also glued with epoxy. The natural frequency of the moving element is related directly to the support-beam stiffness and inversely to the combined mass of the cross-member and grating (McLaughlin, 1977). The effective support-beam stiffness can be varied by attaching the cross-member to the support beams at different heights (*Y* axis; see Fig. 4*B*), in effect changing the length of the beams that serve as cantilevers (i.e., stiffness is inversely proportional to cantilever length). The mass of the moving element is minimized by using the shortest cross-member and the smallest grating permitted by the transducer construction design. The support beams as well as cross-member are small glass rectangular tubing (Vitro Dynamics, Rockaway, NJ), as opposed to the circular glass tubing used in the original design. This change in transducer construction was necessary to eliminate a second stray resonance that was detected in addition to the natural resonance of the circular tubing support beams along the axis of the cross-member (*X* axis). Since circular tubing can bend equally in all directions, we deduced that the stray resonance was probably related to a lateral motion of the glass rods (*Z* axis; see Fig. 4*B*). The rectangular tubing (height-to-width ratio: 1:10) is relatively resistant to motion perpendicular to the plane of its short side, and thus might be expected to eliminate lateral movement of the moving element.

The light source is a quartz-halogen lamp (bulb EJL; Sylvania/GTE, Warren, PA) powered by a precision-regulated 24-V DC power supply (Sorensen Co., [Raytheon Co.], Manchester, NH). The light passes through a series of infrared filters and mirrors (Melles Griot, Irvine, CA) to minimize thermal effects on the grating and then enters a fiber optics bundle (Dolan-Jenner Industries, Inc., Woburn, MA). The fiber optics bundle bifurcates into two smaller bundles. The light from one bundle passes through a fixed-grating, moveable-grating collecting

lens, and finally strikes a photodiode, all of which are mounted within the force transducer. The light from the other bundle enters a pair of reference gratings that are fixed with respect to each other. The output from the transducer and reference photodiodes are connected to a differential amplifier (model 3A9; Tektronix, Inc., Beaverton, OR) to minimize the noise inherent within the bulb. The reference gratings and photodiode are in the present design an independent unit removed from the transducer housing (Canaday and Fay, 1976). By removing the reference unit, the weight of the entire force transducer has been greatly reduced, thereby minimizing a major source of noise resulting from the mass of the force transducer vibrating at the end of the micromanipulator (Fig. 2).

To maximize force transducer sensitivity, the relative spatial orientation of the moveable and fixed gratings must be precisely controlled as previously discussed (Canaday and Fay, 1976). Specifically, the distance between the two gratings and the parallel alignment of the lines between gratings are both crucial for obtaining maximum sensitivity. To facilitate proper positioning of the gratings, the following improvements were made to the new transducer: (*a*) the fiber optics bundle was mounted on a ball-bearing slide (Fig. 4*A*), so that the fixed

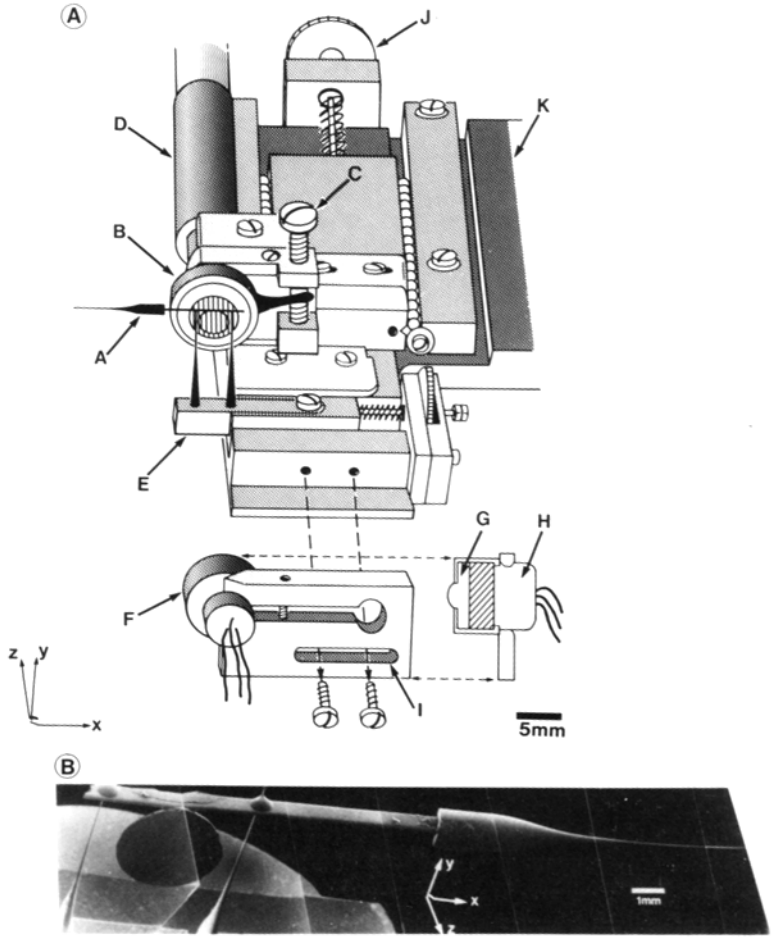

grating at the bundle's end could be positioned to within 0.1 mm of the moveable grating; (*b*) to ensure parallel alignment of the lines between gratings, the fixed grating was epoxied to a rotatable holder so that orientation of the lines on the fixed grating could be properly matched relative to the lines on the moveable grating. To further enhance the transducer sensitivity, the efficiency of light collection by the photodiode was improved by using a plano-convex lens (Klinger Scientific Corp., Richmond Hill, NY; fd = 2 mm, OD = 4 mm) placed one focal length in front of the photodiode in order to focus the light emerging from the gratings onto the diode-sensing area (SGD-100A; EG&G, Inc., Electro-Optics Div., Salem, MA).

At the end of every experiment, the force transducer was calibrated. A meter movement (Canaday and Fay, 1976) was converted into a calibration unit with the amount of current applied to the meter coil related to the amount of force required to prevent the meter arm from moving. By placing the meter arm against the moving element of the transducer and generating a range of forces in the meter arm, the transducer compliance and sensitivity were determined. To calculate the damping time constant and effective mass of the transducer-moving element, the response to an impulse input was recorded with the transducer microprobe positioned in solution as during the experiment. To produce the impulse input, a spring-loaded plunger fixed to the micromanipulator, which supports the force transducer, was pulled back a given distance and

---

FIGURE 4. (*opposite*) Force transducer. (*A*) The new design for the ultrasensitive force transducer (FT) is illustrated. A single SMC is attached to the FT moving-element (A) (see *B*) cross-member, which supports the circular glass Ronchi-ruled grating. This moveable grating is positioned in front of a fixed grating that is mounted on a rotatable holder (B) at the end of a fiber optics bundle (D). Since FT sensitivity is maximized by parallel alignment of the lines between gratings, the ability to match the alignment of the grating lines is obtained by adjusting the screw (C) to raise or lower the black connecting arm of B. Close proximity of the two gratings is also necessary for increased FT sensitivity. Therefore, B is mounted on a ball-bearing slide that is attached to a spring-loaded screw mechanism (J) for fine positioning. To ensure that the moveable grating encounters the entire beam of light emanating from the fiber optics bundle, the moving element is mounted on a spring-loaded slide (E). Light passing through the two gratings is collected by a plano-convex lens (F, G) placed one focal length in front of the photodiode (H) that records the changes in light intensity related to cell force. The position of H relative to the beam of light is adjusted by moving the H holder along its slots (I). The entire FT is constructed of aluminum and is mounted on a micromanipulator at K. (*B*) Scanning electron micrograph montage of the FT moving element. A single SMC is attached to the microprobe tip during an experiment. The microprobe is supported by a rectangular glass rod at the other end of which is epoxied a circular Ronchi-ruled grating. Upon contraction, the cell tugs the moving element along the *X* axis, bending the two vertical support beams that support the cross-member. The transducer stiffness is dependent upon the height (*Y* axis) at which the cross-member is attached to the vertical beams. Calibration bar, 1 mm.

released, striking a plate on the micromanipulator (see Fig. 2). This set the force transducer into resonance at its natural frequency. The resonance amplitude declined to 37% (1/e) of the initial oscillation in a time defined as its damping time constant, Q (Fig. 5*A*). Knowing the transducer's natural frequency and Q, we were able to calculate the transducer's inertial and viscous properties (see Table I). These values were then used to correct for the effect of the transducer's

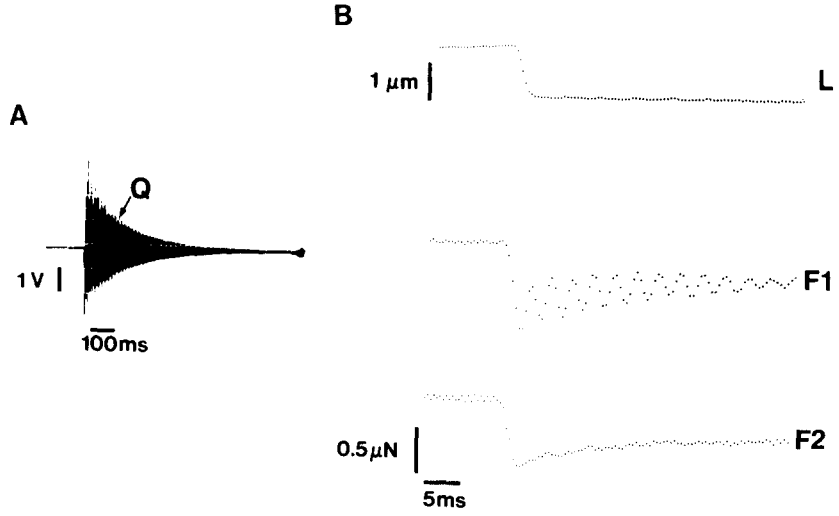

FIGURE 5. (*A*) Determination of damping time constant (Q) for force transducer. To correct the recorded force for inertial and viscous properties of the force transducer (FT), an impulse input of force is imposed upon the FT through a spring-loaded striker (see Fig. 2), allowing one to measure Q. Q is defined as the time for the FT oscillations to decline to 1/e (37%) of its maximum. Knowing Q, FT natural frequency, determined from this record as well, and FT stiffness, a second-order differential equation describing the FT's viscoelastic properties can be used to determine the actual force applied to the FT at all times. Results of this approach are seen in *B*. (*B*) Correction of force data. The tension response to a 0.75% length change at the peak of an isometric contraction was digitized at 2.5 kHz (F1). Knowing the FT's viscoelastic properties, the actual force (F2) applied to the FT at all times can be recovered as described in the text. All force traces to be presented have been similarly treated. Notice that the oscillations in the force record are eliminated after correction of the FT output for the distortion due to the FT inertial and viscous properties. L_{cell} = 175 μm; diam = 3.5 μm; F_{max} = 2.14 μN.

inertia and viscosity in order to determine the actual force (Fig. 5*B*) being applied to the transducer at all times, assuming that the transducer's response is that of a viscoelastic system described by a second-order differential equation (Ford et al., 1977; Guth et al., 1979).

Length Controller and Monitoring Systems

Cell length was altered by either a rapid (1 ms), short-range (0–5 μm) device or

a slower (50 ms) system producing longer-range length changes (1–50 μm). The short-range system consisted of a piezoelectric translator (PI-70; Physik Instrumente GmbH & Co., Waldbronn, Federal Republic of Germany; f_n = 1 kHz), onto which the glass microprobe was fixed. The piezoelectric translator was driven by a high-voltage operational amplifier (HV-70; Burleigh Instruments Inc., Fishers, NY), which amplified a computer-generated half cosine wave (0–180°), which was the form for all length steps. Therefore, by varying the amplitude and frequency of the half cosine wave, length steps of varying amplitude and duration were obtained. The resulting length displacement was monitored by an eddy current sensor (KD2300-.5SU; Kaman Instrumentation Corp., Colorado Springs, CO) having the following characteristics: f_n = 5 kHz; resolution = 0.03 μm. The displacement sensor required a metallic target at least 2 mm in diameter to record motion accurately, and because of the minute size of the preparation, the motion target was attached at the junction of the piezoelectric translator and glass microprobe (Fig. 2). The target was, therefore, at least 2 cm from the end of the cell. A series of tests was performed to determine: (*a*) whether recording the motion of a target a distance away from the preparation was a true representation of the motion transferred from the translator along a glass microprobe to the cell; (*b*) whether the imposed length change was directed

TABLE I

Typical Force Transducer Properties

Characteristic	
Sensitivity	18 mV/μN
Natural frequency	377 Hz
Damping time constant	96 ms
Compliance	0.09 μm/μN
Effective mass (with microprobe)	2 mg
Long-term drift	0.001 μN/s

along the cell's long axis. By placing a tiny aluminum cube at the end of the microprobe where normally a cell would be attached, a displacement sensor could monitor the motion at the end of the probe. Depending on which face of the cube the sensor was aimed at, motion in the *X*, *Y*, or *Z* axis was monitored. Notice in Fig. 6*A* that the motion of the piezoelectric translator was almost entirely along what would normally be the cell's long axis (*X* axis) and was identical to that normally recorded 2 cm away from the cell attachment. Although slight motion was detected in both the *Y* and *Z* axis, it was no more than 2% of the length change along the cell's long axis. A second test of the uniaxial nature of the translator relied upon the analysis of a double-exposure image of the microprobe just before and upon completion of the length step. Fig. 6*B* demonstrates that in fact the imposed length step was truly uniaxial. This photograph, coupled with the results of the displacement sensor tests, confirmed that monitoring cell length changes 2 cm from the cell end yielded an accurate measure of the imposed length change and that the translator produced length changes that were directed almost completely along the long axis of the cell.

In addition to rapid, short-range length steps, longer-length changes (50 μm in 50 ms) were performed in the following manner. The piezoelectric translator to which the cell was attached was mounted on the arm of a de Fonbrune

(Arenberg Sage Inc., Boston, MA) pneumatic micromanipulator (Fig. 2). The micromanipulator consists of three bellows coupled to individual diaphragms that produce motion in the *X*, *Y*, and *Z* axes. By inserting a three-way stopcock

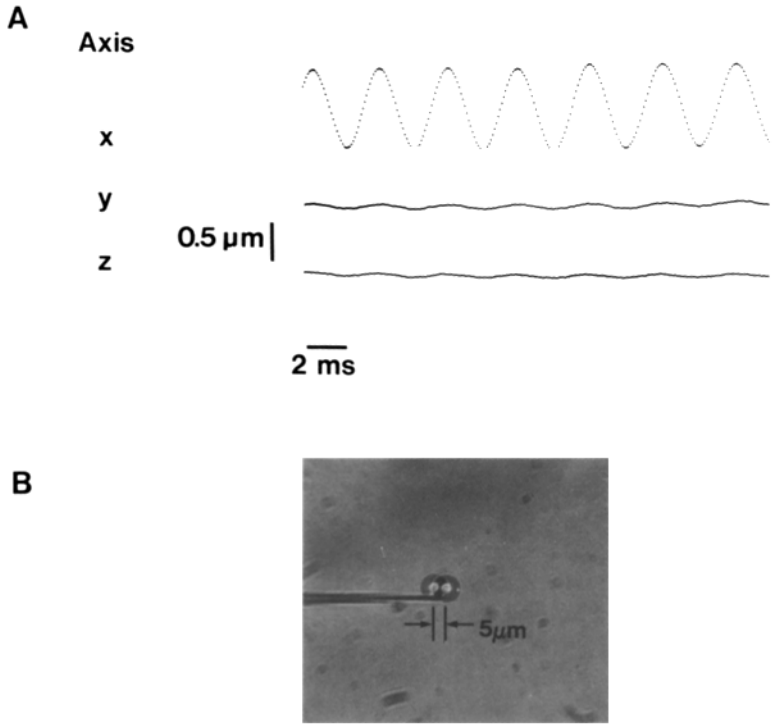

FIGURE 6. Assessment of the uniaxial nature of displacements imposed by the piezoelectric translator. (*A*) Length displacement as monitored triaxially with an eddy current sensor. To assess the uniaxial nature of the length displacement, a tiny aluminum cube was fixed to the very tip of the microprobe to which normally a cell would be attached. The displacement of the cube was monitored by an eddy current displacement sensor aimed at the cube face, corresponding to either the *X*, *Y*, or *Z* axis. The 1.0-μm, 250-Hz displacement that was generated by the piezoelectric displacement device was detected predominantly along the *X* axis with motion in both the *Y* and *Z* axes being no more than 2% of that along the *X* axis. Sensor signal was filtered with a 1-kHz low-pass filter to improve signal-to-noise ratio (10:1). (*B*) A double-exposure image of the bead at the microprobe's end was obtained just before and immediately after a length change of 5 μm in 2 ms. Notice that no lateral displacement is observed, which confirms the results in Fig. 6*A* indicating that the imposed length changes are truly along the cell's long axis.

into the air line connecting the *X*-axis diaphragm to its hand-operated (i.e., joystick) bellows, a 50-ml syringe could then act as a second bellows to the diaphragm. Small volume changes in the syringe, which in turn displaced the piezoelectric translator and cell, were obtained by a motor-driven micrometer

(model 1207S; David Kopf Instruments, Tujunga, CA) attached to the syringe plunger.

In our efforts to eliminate all sources of mechanical vibrations within the entire recording system, a series of tests (see SYSTEM'S NOISE ANALYSIS below) revealed the presence of vibrations in the diaphragm of the micromanipulator. These were particularly severe during the length changes when an equal and opposite reaction in response to the rapid motion of the piezoelectric translator was initiated in the micromanipulator diaphragm. These mechanical vibrations were directly transmitted to the cell through the coupling of the micromanipulator and the piezoelectric translator. An oil damper (see Fig. 2) was therefore designed and constructed to eliminate these reactions.

Mock Cell Data

Before interpreting the tension transients as a reflection of cellular responses, the force transducer's ability to record force accurately had to be assessed. To rule out any possibility of the transients being an artifact of the force transducer, a material of known elastic characteristics was attached between the force transducer and the displacement device in an identical manner to that used for the SMC. The test forces measured were in a range comparable to the forces that one would expect from a muscle cell.

The test material was rubber cement formed into fine strands with dimensions similar to that of a cell. The fine thread of rubber cement was initially attached to the beads on both microprobes while still tacky, much like a cell. After tying the mock cell around the microprobes as we would an SMC, a series of tests identical to those employed during cellular experiments was imposed. Fig. 7 is a comparison of tension transients resulting from a rapid change in the length of a single SMC and a mock cell. Notice that both the SMC and mock cell responded to the length change with a coincident tension change; however, the new tension level was not maintained in the SMC and in fact finally recovered to its initial value. On the other hand, the mock cell did not exhibit appreciable recovery, which suggests that the recovery observed in the SMC was not an artifact of the transducer but most likely a cellular process. The appearance of a slight recovery for the mock cell (23%) was most likely due to the long-term viscoelastic behavior of rubber cement, as it was not seen with glass threads interconnecting the force transducer and length driver. To characterize further the recording capabilities of the force transducer, a series of stretches and releases either of constant duration but variable amplitude or of fixed amplitude but variable time for completion was applied to the mock cell. If the material being tested possessed linear elastic characteristics, then the stiffness ($\Delta F/\Delta L$ = slope of instantaneous length:force relationship) should have been independent of the amplitude and speed of the step. In Fig. 8*A* and *B*, instantaneous force is plotted against length during the step and, as predicted, the length:force relationships (L:F) for each series of tests superimpose, which indicates that the force transducer can accurately record at frequencies up to 400 Hz the force response of a rubber mock cell with known elastic properties.

The tests just described involved determination of stiffness from transients at one particular level of force. As several studies involve determination of stiffness of our cells at various levels of force, we investigated whether the determination of stiffness from transients of a standard test material was dependent upon the level of force at which the tests were initiated. One would predict that for a

linear elastic material, regardless of the force exerted by the material, stiffness should be independent of force. Although a rubber cement cell satisfied our test criteria for a material with short-range (<1.0% ΔL) linear characteristics that could be knotted as would a cell, the long-range behavior of rubber cement was rather exponential. Having an exponential stiffness, the measured stiffness would vary directly with the force exerted by the material rather than being independent of it. To avoid this problem, a fine glass thread was drawn and epoxied perpendicularly as a cantilever between the force transducer and displacement probes. Glass does possess a linear elasticity and, therefore, bending the glass

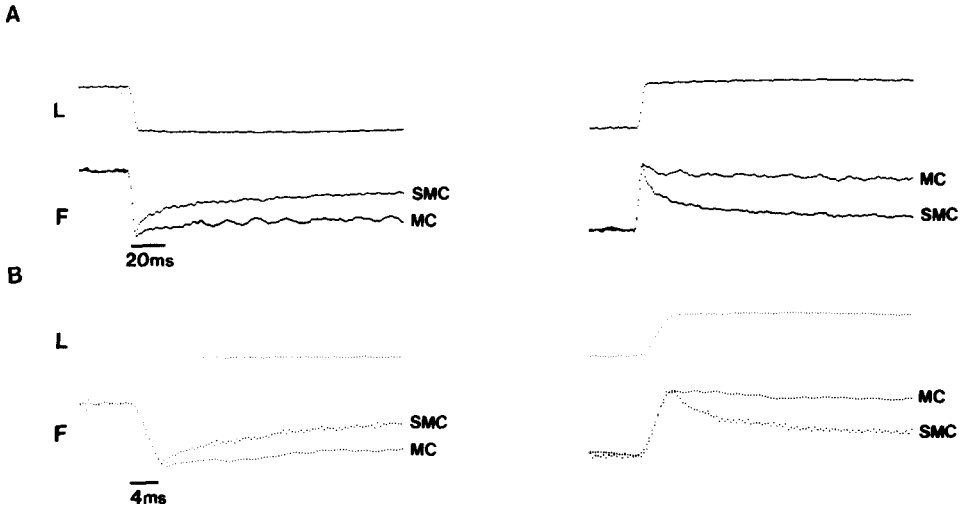

FIGURE 7. Comparison of tension transients in a rubber mock cell vs. a single smooth muscle cell. To test whether the tension transients do in fact originate within the SMC, a fine rubber mock cell (MC) (L = 100 μm × 6 μm diam) was attached to the force transducer and displacement device in a manner similar to that used for an SMC. Notice that in response to either a decrease (left) or increase (right) in length there is little recovery (≈23%) after 100 ms as opposed to 73% recovery in the SMC. Calibration bars have been omitted because the tension responses are normalized values. The tension transients shown in *B* are the same as those in *A*, but at a four-times-faster time scale. Note that within this time frame virtually no recovery is observed in the MC.

beam by various amounts resulted in different levels of force. Fig. 8*C* shows the L:F from transients obtained from a glass thread at two different force levels. Notice that the stiffnesses were independent of the force level as would be expected. These results, together with the previous mock cell experiments, indicated that the force transducer could faithfully record over a wide range of forces transients in response to length changes of various rates (≤400 Hz) and amplitudes, and that the stiffness determined from such measurements was an accurate measure of the properties of that material.

Computer-assisted Protocols and Data Analysis

A small laboratory computer (LSI-11/23; Digital Equipment Corp., Marlboro,

MA) with both analog-to-digital and digital-to-analog conversion capabilities was used for length control, timing purposes, and spectral analysis of data. Both length and force records were stored on FM tape and analyzed on a larger computer (PDP-11/40; Digital Equipment Corp.) with greater storage capacity.

LENGTH CONTROL AND EXPERIMENTAL PROTOCOLS Programs to control and vary cell length were developed. As seen in Fig. 9*A*, a series of computer-generated length changes was first imposed while the cell was relaxed. The cell was then electrically stimulated to contract, and at the peak of contraction an identical series of length changes was imposed. The following protocols used in our study follow this general sequence of events; therefore, only a description of the amplitude and rate of the length steps will follow.

Stiffness During the Development of Force. This protocol served to determine how cell stiffness varied as force was being generated. Therefore, steps of 0.5% cell length (2.0 ms duration) were imposed continuously at 1-s intervals as the cell went from the relaxed state to the peak of force generation (see Fig. 18).

Varying Amplitude Length Steps. To investigate the length dependence for all phases of the tension transient, various amplitude length changes were imposed. This protocol involved a series of six pairs of step releases and stretches (0.5, 0.1, 0.3, 0.5, 1.0, and 0.5% each step complete in 2.0 ms) having a 1-s interval between steps (Fig. 9*B*). The 0.5% length change served as an internal control for possible fatigue or degeneration of the fiber as might be indicated by substantial changes in the form of the transient that may have occurred throughout the series of steps. This series was performed at rest and at the peak of contraction.

Varying Time for Completion of the Step. This protocol was designed to determine whether the speed of the length step could alter the form of the tension transient. The timing is similar to the previous protocol, except a constant amplitude of 0.75% cell length was imposed having the following times for completion of the step: 5.0, 1.7, 2.5, 5.0, 10, 25, and 5.0 ms (Fig. 9*C*). In this series the 5.0-ms step served as the internal control for fiber fatigue and degeneration.

DOUBLE-EXPOSURE FLASH PHOTOGRAPHS As described earlier, double-exposure images of the length microprobe were used to confirm that the imposed length steps were directed along the cell's longitudinal axis. This technique was also used to determine if the length change was distributed uniformly along the cell. We addressed this question by decorating cells with tiny (1 μm diam) anionic exchange resin beads and obtained double-exposure images of these cells just before and immediately after the length step. By measuring the distance between edges of the bead's double image, the extent of cellular displacement in response to the step was determined at the various bead locations. To obtain double exposures with high time resolution, a high-intensity xenon arc flash unit (Strobex; Chadwick-Helmuth Co., El Monte, CA) having a recharge time of 40 ms and a flash duration of 20 μs was used to expose 35-mm film (ASA 125). It was crucial that the length step, double-exposure flash, camera shutter, and film advance all be properly timed and coordinated. Double-exposure photographs were obtained under computer control with the following sequence of events: (*a*) The camera shutter was opened using a pneumatically driven plunger to depress the shutter release, which was held open between flashes by maintaining the air pressure into the plunger using a computer-triggered electromagnetic pneumatic valve (model EV-3; Clippard, Cincinnati, OH). (*b*) The first flash was triggered 100 ms before the step. (*c*) The length step was applied to the cell. (*d*) The second flash was triggered 15 ms after completion of the step. (*e*) The

A

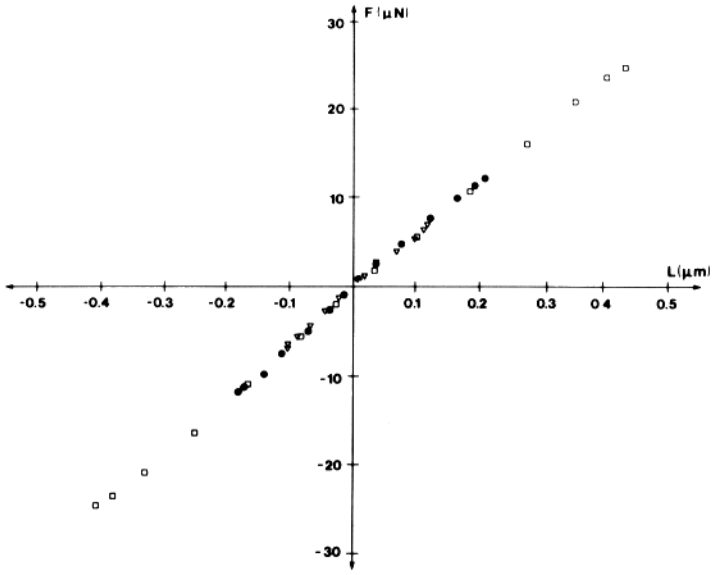
F (μN)
30
20
10
-10
-20
-30
L(μm)
-0.5
-0.4
-0.3
-0.2
-0.1
0.1
0.2
0.3
0.4
0.5

B

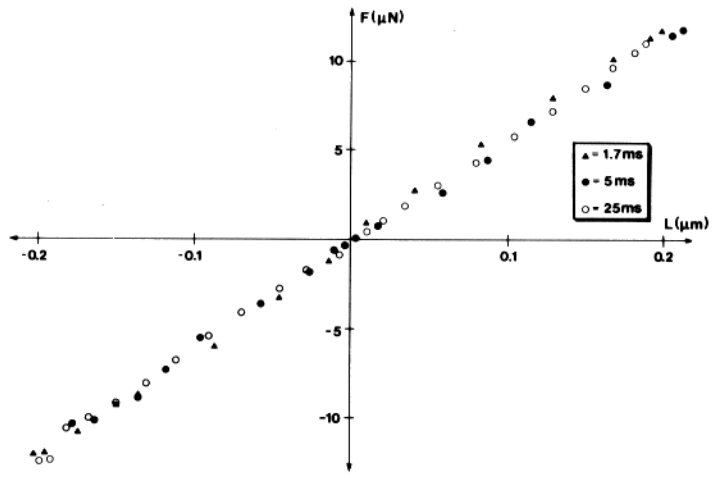
F(μN)
10
5
-5
-10
▲ = 1.7ms
● = 5ms
○ = 25ms
L(μm)
-0.2
-0.1
0.1
0.2

C

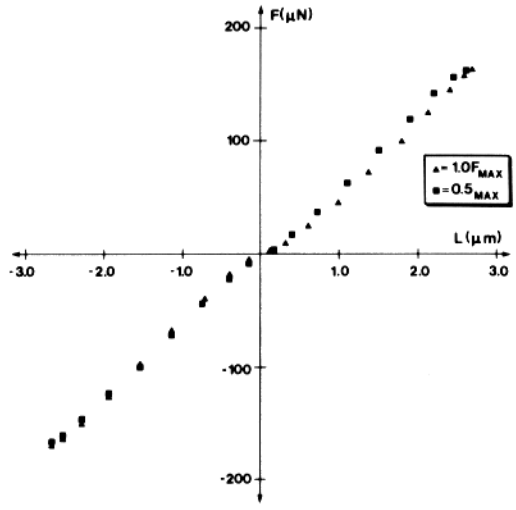
F(μN)
200
100
-100
-200
▲ = 1.0F MAX
● = 0.5 MAX
L(μm)
-3.0
-2.0
-1.0
1.0
2.0
3.0

camera film was automatically advanced using an electronic film drive (Carl Zeiss, Inc.). The resulting images are shown in Fig. 10*A* and *B*.

SYSTEM'S NOISE ANALYSIS Since typical tension changes that were recorded in response to length steps were as small as 0.1 μN, it was imperative that noise within the recording system, either of electronic or mechanical origin, be reduced well below this level. To track down the sources of such noise, a spectral analysis program was used to analyze either the output of the force transducer for both electronic and mechanical noise or the output of an eddy current displacement sensor that monitored minute mechanical vibrations of component parts within the recording system. Therefore, with no cell attached to the recording system, the apparent noise in the force and displacement signals were analyzed in terms of their amplitude and frequency spectrum. By comparing noise spectra before and after an instrument in the laboratory was turned off, the precise amplitude and frequency of that instrument's contribution to the overall noise could be determined (Fig. 11). By repeating this test for all instruments, sources of noise in the entire system were characterized. Measures were then taken to alleviate or minimize the noise and, as a result, the noise in the force transducer output was no greater than 0.005 μN peak to peak.

Solutions

All experiments were performed at room temperature (20°C) in amphibian physiological saline (APS). APS was composed of the following concentrations (mM): 108.9 NaCl; 3.0 KCl; 20.0 $NaHCO_3$; 0.1 NaH_2PO_4; 0.6 $NaHPO_4$; 1.0 $MgSO_4$; 1.8 $CaCl_2$; 0.2% glucose. This solution was continuously bubbled with 95% O_2/5% CO_2 to pH 7.4.

FIGURE 8. (*opposite*) (*A*) Length:force relationships for mock rubber cell obtained from length steps of various amplitudes. The length:force relationship (L:F) was obtained from data in Fig. 7 analyzing the variation in force (F) during the length step (L). Releases ($-L$) and stretches ($+L$) of various amplitudes (∇ = 0.1%; ● = 0.2%; □ = 0.4%) were completed in 2 ms. Notice that the L:F is linear and independent of the step amplitude. These results suggest that the force transducer is capable of accurately recording force from a material of known elastic properties over a range of forces (30 μN) at a frequency of 400 Hz. $L_{\text{mock cell}}$ = 100 μm; diam = 6 μm. (*B*) Length:force relationship for mock cell obtained from length steps of constant amplitude but various speeds. A constant-amplitude length step (0.2%) with various times for completion of the step was imposed. Notice that all L:F superimpose, which suggests that the elastic mock cell has no viscous recovery over this short range of length. Furthermore, note that the stiffness is identical to that obtained in Fig. 7*A* using various amplitude steps, which indicates the ability of the FT to accurately follow changes in force as rapid as 400 Hz. (*C*) Length:force relationship of glass cantilever obtained at two force levels. A glass thread was attached as a cantilever between the force transducer and the displacement device. Small, 0.1% length steps were applied (complete in 2 ms) at two different force levels. The various force levels were obtained by bending the cantilever before applying the small length steps. Notice that the L:F is linear and independent of the force level, as would be expected from a material with a linear elasticity. L_{glass} = 5 mm; $\text{diam}_{\text{glass}}$ = 41 μm; F_{max} = 1 N.

RESULTS

Isometric Force Production

The time course for SMC isometric force production in response to electrical stimulation appears in Figs. 9*A* and 18. These cells typically reach peak force in ~7 s at 20°C. Table II lists both the cellular dimensions as well as values for several mechanical properties observed

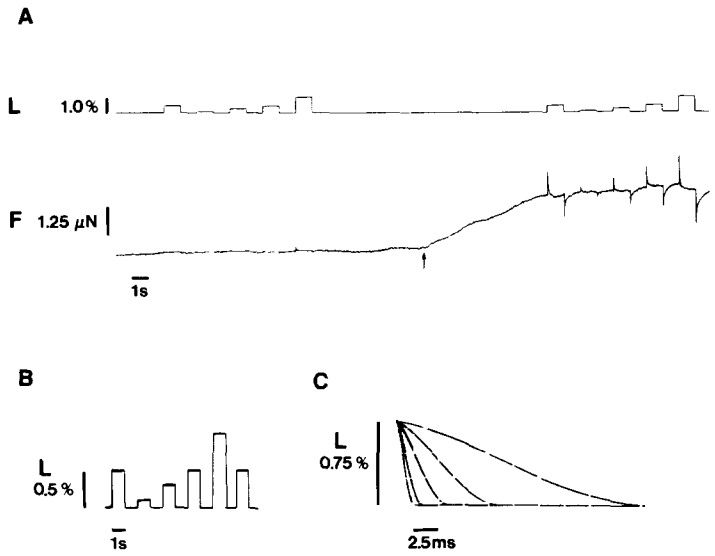

FIGURE 9. (*A*) Typical isometric contraction of a single smooth muscle cell and experimental protocol for eliciting isometric transients. A series of various amplitude length steps was imposed in the relaxed state and at peak isometric force. The cell was stimulated to contract at the arrow. Notice that the tension responses in the relaxed state are negligible, but are apparent during active contraction. L_{cell} = 176 μm; diam = 5 μm. (*B*) Varying amplitude protocol. The following sequence of length steps was applied to assess the amplitude dependence of the tension transients: 0.5, 0.1, 0.3, 0.5, 1.0, and 0.5%. All steps are complete in 2 ms and are maintained for 1 s. (*C*) Varying rate of length step protocol. The following sequence of constant-amplitude (0.75% L_{cell}) length steps of various durations for completion of the step was applied to assess the dependence of the tension transients on the speed of the applied length step: 5, 1.7, 2.5, 5, 10, 25, and 5 ms. Each step is maintained for 1 s.

in this study. In addition, mechanical properties from both smooth muscle tissue and single skeletal muscle fibers are listed for comparison with the single SMC.

Just before activation, a series of various amplitude length steps was imposed. Notice that no detectable change in force in response to the steps was observed while the cell was relaxed. Figs. 12 and 13 demonstrate that the transients observed during the relaxed state are negligible and

comparable to the noise of the force recording system. In contrast to the relaxed muscle, tension transients are readily apparent during active force generation. The experimental protocol of rapid length steps had no effect upon the time course of force generation or the maximum steady state force (see Figs. 9*A* and 18).

Tension Transients

GENERAL CHARACTERISTICS The tension transients recorded from SMC in response to various amplitude length steps (0.3 → 1.0% L_{cell}) complete in 2.0 ms are presented in Figs. 12 and 13. All transients possess characteristic features that are described as follows:

(*a*) An immediate rise or fall in tension that is coincident with the imposed increase or decrease in cell length.

(*b*) A rapid recovery of tension that occurs during the length step, the presence of which is evident as force reaches its maximum tension change and in fact begins to recover before completion of the length step (Fig. 16*C*).

(*c*) Upon completion of the length step, a further recovery of tension to its initial level before the step, within 1 s. This recovery could be resolved mathematically into two components. If one plots the logarithm of percent recovery vs. time after completion of the step (Warshaw and Fay, 1983*b*), the presence of both a fast (τ_{fast} = 5–20 ms) and slow (τ_{slow} = 50–300 ms) exponential recovery process becomes readily apparent.

Tension Transients Related to Active State

The lack of tension transients in relaxed cells and the appearance of transients upon contraction suggest that the structures whose mechanical properties are being probed are recruited upon activation. To test further whether the transients reflect mechanical properties of structural elements responsible for the ability of SMC to actively produce force or shorten, two altered cellular models were investigated: (*a*) the glutaraldehyde-fixed cell; (*b*) the rigor-like supramaximally contracted exhausted cell. To study a glutaraldehyde-fixed cell (Kawai et al., 1977), a push-pull perfusion system (Harvard Apparatus Co., Inc., South Natick, MA) was employed. The perfusion pipette was placed within 5 mm of the cell, allowing the fixative front (2% glutaraldehyde, 3.0 ml/min) to engulf the cell within 1 s. Before and during fixation a sinusoidal length perturbation (0.5% cell length, 230 Hz) was imposed with the amplitude of the sinusoidal force response an index of cell stiffness. During fixation, force rose to 0.62 F_{max} with a stiffness-to-force ratio two times greater than in an actively contracted cell. Once fixation was complete (i.e., 20 s), a series of various amplitude length changes of constant duration, as well as a series of steps of various durations but constant amplitude, was imposed. The most obvious difference of the tension transients in the glutaraldehyde-fixed SMC was the lack of recovery normally observed in contracting SMC (Fig. 14). The relationship between the force and length during the

length change was linear and independent of either the amplitude or rate of the step. This suggests that a fixed cell behaved like the rubber mock cell, having truly linear instantaneous elastic properties, and in addition there was no recovery.

The second smooth muscle preparation having an altered contractile state was the exhausted rigor-like cell. After a supramaximal electrical stimulation, cells would maximally contract for periods >60 s. At that time, in response to a large release in length (>10%), the cell could no longer shorten as judged by its inability to fully redevelop force. Since the cells appeared to be in a rigor-like state, we imposed small (<1%) length steps to such cells. Notice that the recovery has been markedly

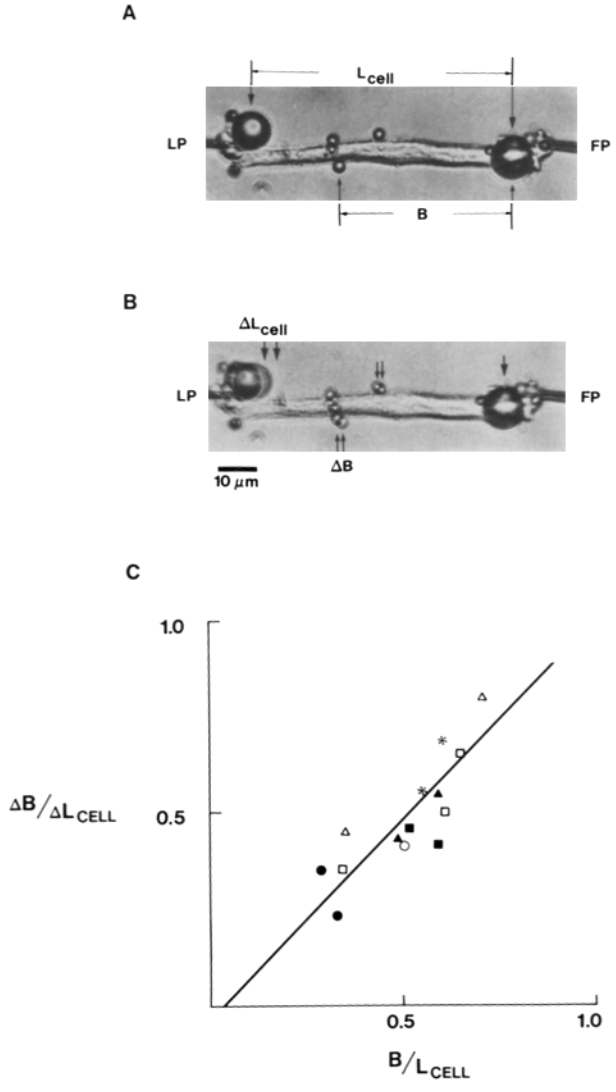

diminished as compared with the active cell much like that in the fixed and mock cells (Fig. 14). The fact that transients are not apparent in the relaxed cell and differences in their form exist in SMC having an altered contractile state suggests that tension recovery is due to cellular structures responsible for active force generation and cell shortening.

Double-Exposure Flash Photographs

The mock, resting, and altered cell data suggest that the form of the tension transients is unique to an actively contracting cell. Therefore, the transients must reflect the response to a sudden change in the length of structures within the cell that are involved in force production and cell shortening. The contractile filaments, presumably central to force production, are distributed throughout the entire cell and are likely candidates for the structure being probed. If this is the case, then the imposed length change must be distributed uniformly along the entire length of the cell to ensure that the length step has been applied to all the contractile material and that the resulting tension response adequately reflects its properties. Alternatively, the response might be dominated by the knotted ends of the cell. If the knots represent areas of high compliance, they would absorb most of the length step and therefore most of the tension response might be expected to arise from the length change in this local region.

FIGURE 10. (*opposite*) Determination of the distribution of a length change applied at the end of a smooth muscle cell over the length of a cell. (*A*) Photomicrograph of an SMC with adherent anionic exchange resin beads. A single SMC was tied to the microprobes that are connected to the force transducer (FP) and length displacement device (LP). To determine whether the length step is uniformly distributed along the entire length of the cell, tiny anionic exchange resin beads were added to the solution in which the cell was bathed and some adhered to the cell surface. Such cells were stimulated and a length step was imposed. A double-exposure photograph was obtained before and immediately after the step (see *B*). The cell length (L_{cell}) and position of the bead (B) from the fixed end of the cell (i.e., FP) are measured. (*B*) Double-exposure flash photomicrograph of a single smooth muscle cell before and just after an applied length step. A double-exposure flash photograph was taken 100 ms before and 15 ms after the length step (ΔL_{cell}). Motion at points along the cell occurring as a consequence of the length step is measured as the distance between bead double images (ΔB). (*C*) Relative movement of beads on cell surface after a step. The motion of each bead is expressed relative to the overall length change applied to the cell (Y axis), as is the bead position along the cell (X axis). Data shown are for seven cells. The linear regression line of the following equation is plotted: $\Delta B/\Delta L_{cell} = 1.01\ B/L_{cell} - 0.03$; ($r^2 = 0.73$). The direct relationship between relative bead displacement and relative bead position suggests that the length step is uniformly distributed along the cell's length and argues against the existence of regions of high compliance in the cell's knotted ends.

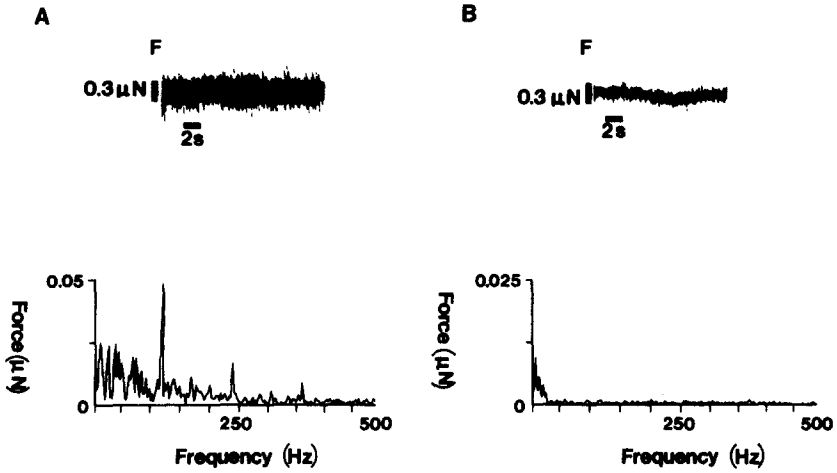

FIGURE 11. Spectral analysis of force transducer output and reduction of system noise. (*A*) Before noise reduction, the output of the force transducer (F) was subject to Fourier analysis to determine the amplitude of noise at frequencies between 0 and 500 Hz. The noise frequency distribution aided in assessing the sources of the noise and in subsequently reducing the noise level. (*B*) After turning the room lights and halogen lamp fan off, a significant reduction in recorded noise (F) is obtained. Notice that the amplitude:frequency spectrum is greatly diminished. Using this analysis, all sources of noise were detected, giving a final noise level of 0.005 μN peak to peak within the frequency range 0–500 Hz.

TABLE II

Single Smooth Muscle Cell Data

Characteristic	Units		Comparisons: Whole smooth*	Comparisons: Single striated fiber‡
Length (L_{cell})	μm	137±7 (20)		
Diameter	μm	4.8±0.3 (20)		
Active force (F_{max})	μN	2.26±0.20 (18)		
Active stress (P_{max}) (F_{max}/cross-sectional area)	mN/mm^2	148±23 (18)	190	235
Relaxed Young's modulus (E_{rest})	× 10^4 mN/mm^2	0.035±0.007 (9)	0.040	0.032
Active Young's modulus (E_{act})	× 10^4 mN/mm^2	0.98±0.19 (18)	1.30	4.41
E_{act}/P_{max}		71±6 (18)	46	189
Temperature	°C	20	37	2.5

Values = mean ± SE. Numbers in parenthesis = number of cells. * Warshaw et al., 1979. ‡ Ford et al., 1977.

By using the double-exposure flash photographic system as described earlier, the extent to which the length step is distributed along the cell's length could be determined. The double-exposure photographs (Fig. 10*A*

and *B*) demonstrate that motion can be detected, with the distance between edges of the beads' double image an index of the motion occurring at that bead location. The results from seven cells are plotted in Fig. 10*C* as the movement of each bead relative to the applied length change vs. the relative distance of each bead from the fixed end of the cell (i.e., the end connected to the force transducer). A linear relationship between the percent of length change and the relative bead location is

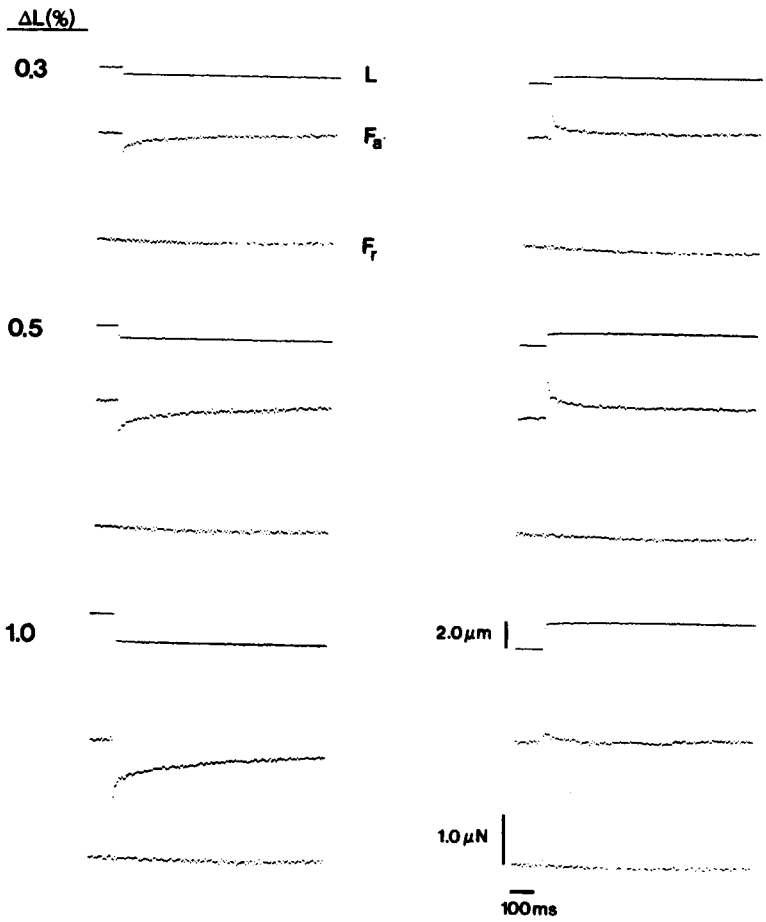

FIGURE 12. Tension transients in a single smooth muscle cell in response to length steps of various amplitudes. At the peak of contraction, a series of various amplitude releases (left) and stretches (right) (complete in 2 ms) was applied. The length (upper trace, L), total active force (middle trace, F_a), and resting force (lower trace, F_r = 0.06 μN) are presented for each amplitude length change. Notice that the tension responses in the relaxed SMC are negligible but are quite apparent during maximum active force production. L_{cell} = 176 μm; diam = 5 μm.

seen, which indicates that no motion is detectable at the cell's fixed end and that progressively greater motions are detected moving toward the end at which the length step is applied. These data suggest that the length change is in fact uniformly distributed and rules out the existence of a significantly high compliance within the knotted region of the cell.

Instantaneous Length vs. Force Characteristics

Since the transients are observed only during active force generation, which presumably involves cross-bridges, the form of the transient may

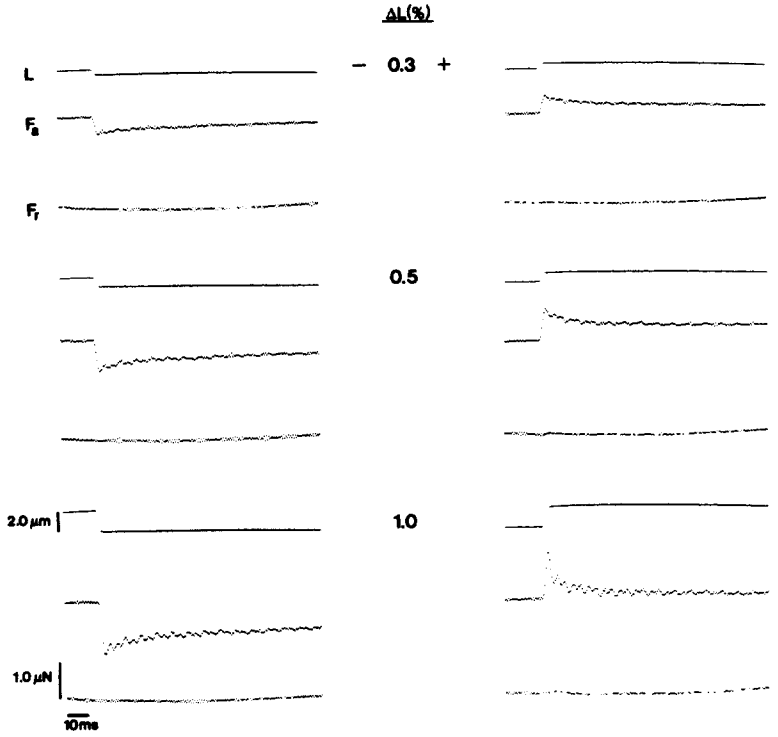

FIGURE 13. Tension transients in response to length steps of various amplitudes at a faster time scale. Responses shown are those from Fig. 12 at a faster time scale.

reflect cross-bridge mechanical and kinetic properties. In striated muscle, the $L{:}F$ is believed to reflect the response of a linear elasticity that resides within the cross-bridge (Ford et al., 1977). When the $L{:}F$ for either releases or stretches in length ($\leq 1.0\%$ L_{cell}) in an SMC at the peak of force production was examined (see Fig. 15), force was observed to vary linearly with length except towards the end of the step where a curvature became apparent. We believe that the nonlinearity reflects a rapid tension recovery that is superimposed upon the elastic response. Note that the time course of the length step follows a half cosine wave so that slowing toward

the end of the step would allow more time for recovery to take place. This contention is supported by inspection of Fig. 16*C*, where force begins to recover before completion of the length step, which is indicative of a rapid process for recovery of tension after the peturbation of steady

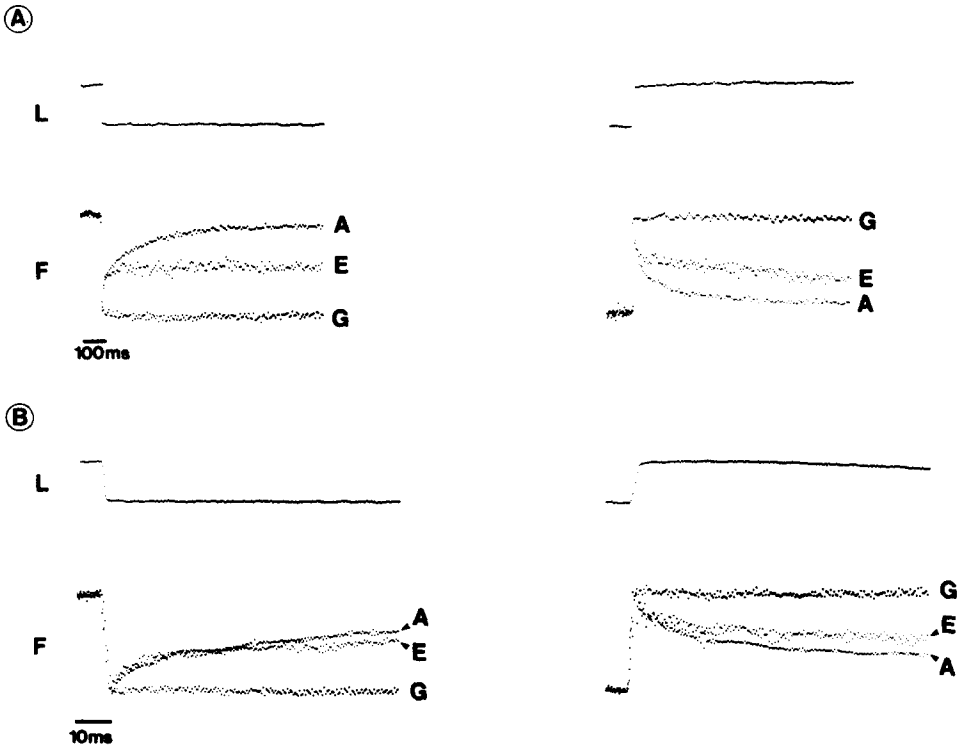

FIGURE 14. Tension transients in three smooth muscle cells in different contractile states. (*A*) Tension transients (F) in responses to either a decrease (left) or increase (right) in cell length (*L*) are presented. The responses from a glutaraldehyde-fixed cell (G) and exhausted rigor-like cell (E) are compared with a tension transient from an actively contracting cell (A). Notice that only in A does complete recovery occur, whereas in E only the initial rapid recovery component exists, and absolutely no recovery is observed in G. No force calibration bars are shown since the tension transients have been normalized for the same initial elastic response. (*B*) Identical transients to those in *A* are shown but at a faster time scale. Notice that fast recovery component still remains in E as in A but is nonexistent in G.

state isometric tension. To more accurately test for the existence of a rapid tension recovery during the step, a series of steps having a constant amplitude but various times for completion was imposed at the peak of contraction (Fig. 16*A* and *B*). One would expect that the faster the step, the less recovery, and the more linear the *L*:*F*. As seen in Fig. 17, the

deviation from linearity between 0.25 and 0.75% L_{cell} observed in the slowest release (25 ms) is considerably reduced in the fastest release (1.7 ms). These data confirm the existence of a rapid tension recovery whose extent is related to the time for completion of the length step. To reduce or eliminate the rapid tension recovery, steps that were 0.5% L_{cell} and complete in 2.5 ms were imposed so that a more accurate reflection of the fiber elasticity could be obtained.

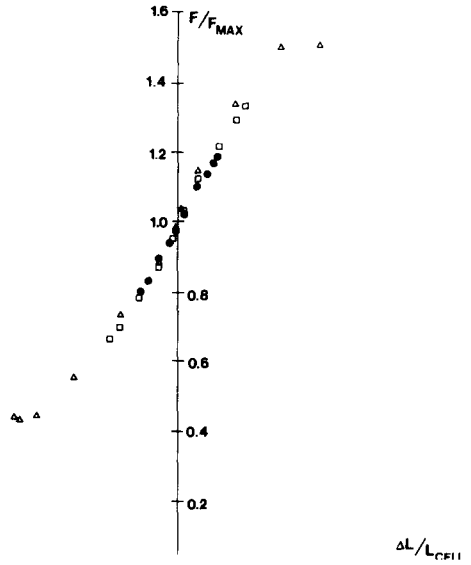

FIGURE 15. Relation of length and force in a single smooth muscle cell during length steps of various amplitudes. At the peak of contraction releases and stretches (complete in 2.0 ms) with the following amplitudes were applied: ● = 0.3%; □ = 0.5%; △ = 1.0%. F and ΔL are expressed relative to maximum force (F_{max}) and cell length (L_{cell}), respectively. Notice the curvature in the relationship at the end of the step, which is believed to reflect the rapid recovery of force that begins during the ΔL itself (see text). Linear extrapolation of the L:F indicates that a ΔL of 1.5% would be required to drop force to zero in this cell. An average value of 1.6 ± 0.2% L_{cell} to drop force to zero is obtained in six cells in which this experiment was performed.

Using these criteria to minimize the tension recovery, a mean value for maximum fiber elasticity (i.e., Young's modulus, E = [(change in tension/cell cross-sectional area) × ($L_{cell}/\Delta L_{cell}$)]) of 1.26 × 10^4 mN/mm^2 was obtained. By extrapolating the linear L:F to zero force, it appears that a 1.6 ± 0.2% (n = 6) length change is required to reduce force within the cell to zero.

As stated earlier, in striated muscle the instantaneous elastic response reflects cross-bridge elasticity. Therefore, the slope of the L:F during the

length step is believed to be a measure of cross-bridge stiffness (Julian and Sollins, 1975). If this is also true in smooth muscle, then upon activation as the numbers of cross-bridges acting in parallel increases and force rises, a proportional increase in fiber stiffness (i.e., the sum of cross-bridge stiffness) should be observed. Therefore, during the development

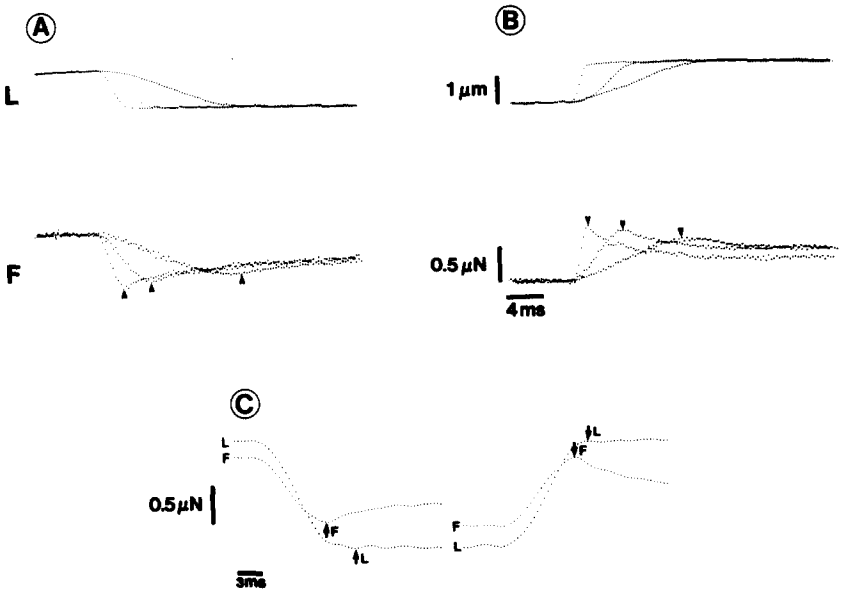

FIGURE 16. Tension transients in a single smooth muscle cell in response to length steps of various speeds. (*A*) At the peak of contraction, 0.75% releases were imposed with the following times for completion (from left to right): 2.5, 10, and 25 ms. Notice that because of the presence of a rapid recovery taking place during the step, a much smaller peak change in force (arrowheads) is obtained as the length change slows, thus allowing more time for recovery. (*B*) As in *A*, 0.75% stretches were imposed with the following times for completion (left to right): 2.5, 10, and 25 ms. As in *A*, peak force responses (arrowheads) are reduced in slower stretches. (*C*) A typical pair of tension transients in response to a release (left) and stretch (right) of 0.75% cell length complete in 5 ms were obtained at the peak of contraction and shown at a fast time scale. Note that maximal force change occurs before completion of the step (arrows) and in fact reverses its direction, which is indicative of a recovery in force during the length step itself. L_{cell} = 175 μm; diam = 3.5 μm; F_{max} = 2.14 μN.

of force upon activation, length steps were imposed (protocol 1) so that a measure of fiber stiffness (*E*) and its relation to force (*F*) could be obtained. This relationship (*E* vs. *F*) is shown in Fig. 18. Notice that stiffness varies in direct proportion to force. A linear regression analysis of the data reveals a slope of 0.85 and an intercept of 0.09 (r^2 = 0.99). This result definitely supports the view that the elastic responses recorded

do originate in cross-bridges that are recruited during force development upon activation.

DISCUSSION

Smooth Muscle Cell Force Production

The use of single SMC as a model for normal smooth muscle contraction is supported by past studies in this laboratory which demonstrated that isolation procedures did not alter SMC function (Fay et al., 1976). Earlier studies also confirmed that the contractile response of these cells was

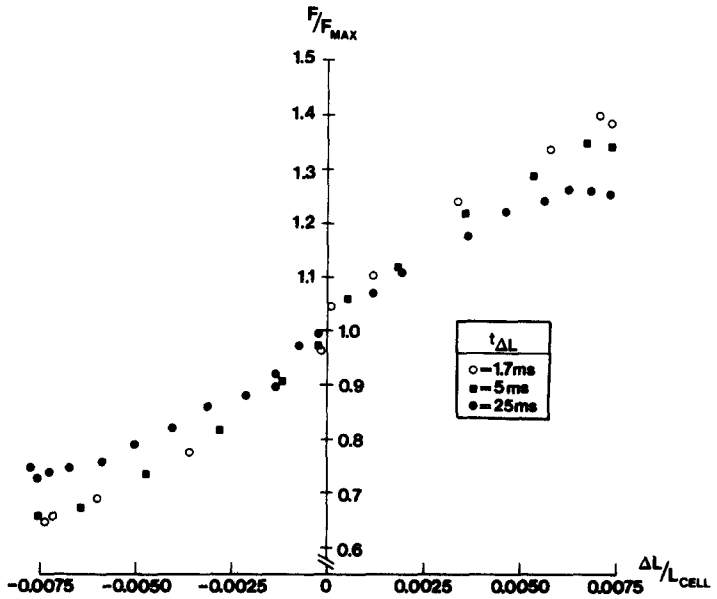

FIGURE 17. Relationship between length and force for a single smooth muscle cell during length steps. Releases and stretches (0.75% L_{cell}) were imposed at the peak of contraction (F_{max}). Data are plotted as in Fig. 15. Notice that the L:F becomes steeper and more linear with faster steps, which suggests the presence of a rapid recovery during the ΔL.

similar in its extent and time course to that of the tissue from which it was isolated (Fay and Singer, 1977). We therefore believe that the results of the present studies are a true reflection of the cellular processes involved in force production as it would be *in situ*. However, the advantage of the single-cell preparation is that direct information about the contractile process is available and is free of the complex interactions between cells and the connective tissue matrix that exist in multicellular preparations (Alexander, 1976; Cox, 1977; Meiss, 1978).

The generation of force in single SMC is maximal at 7 s. This time course does not differ substantially from previous studies in tissue but is

one to two orders of magnitude slower than the speed of force generation recorded in many fast striated muscles. Although the time-to-peak tension is longer in SMC, maximum force production normalized to muscle cross-

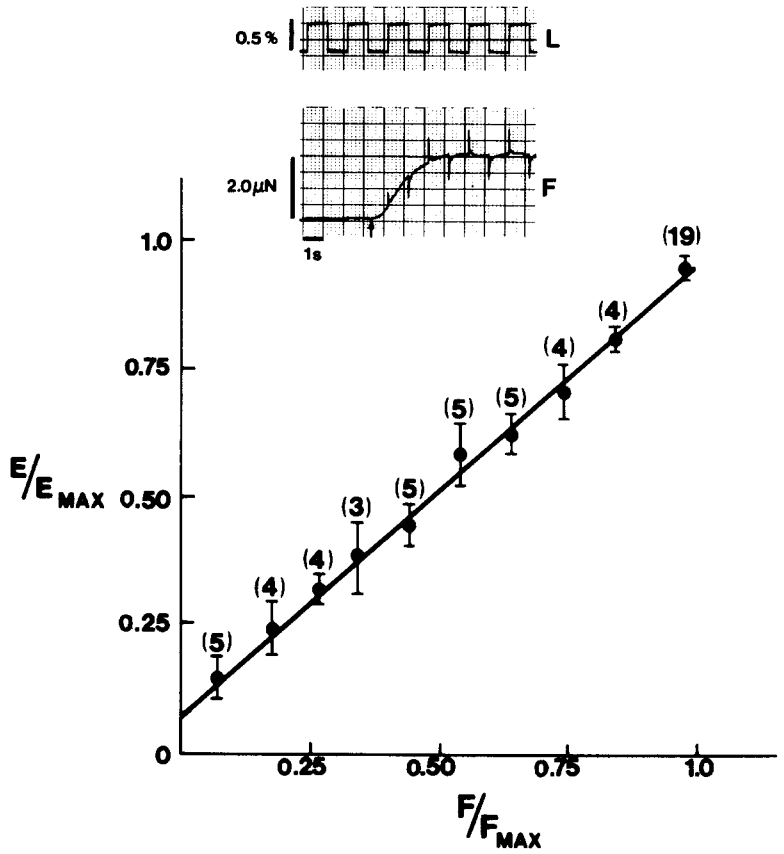

FIGURE 18. Relationship of stiffness (Young's modulus) and force during the development of active force. During the development of force after activation, 0.5% length steps (complete in 2.0 ms) were applied at 1-s intervals (see inset). Stiffness normalized to peak stiffness (E/E_{max}) was determined from the linear portion of the L:F during each length step. Normalized stiffness is plotted against the level of force normalized to the peak force (F/F_{max}) at the time of the length step. Points represent the means and standard errors for the observations made at a particular force level. The numbers of observations are in parenthesis. A linear regression of the form $E/E_{max} = 0.85F/F_{max} + 0.09$ ($r^2 = 0.99$) is drawn through the means. $E_{max} = 1.86 \times 10^4$ mN/mm^2; F_{max}/cross-sectional area = 123 ± 31 mN/mm^2 ($n = 6$).

sectional area (i.e., active stress) is comparable to whole smooth muscle (Warshaw et al., 1979) as well as striated muscle (Ford et al., 1977) (see Table II). This is of considerable interest since it is quite likely that in

our cells, as in mammalian vascular smooth muscle (Cohen and Murphy, 1979), there is only one-quarter the myosin in comparison with striated muscle, but comparable forces per square millimeter are produced. Since the cyclic interaction of the myosin cross-bridge with the actin filament is believed to bring about active force production and cell shortening, the slower velocity of shortening and the need for less myosin in SMC to produce equivalent forces might suggest profound differences in the SMC cross-bridge cycle. Information obtained by analyzing the tension transients may reveal differences in cross-bridge properties that would help to explain smooth muscle's unique physiological contractile characteristics.

Origin of the Elastic Response

To interpret the tension transients in single SMC, let us first consider where these transients originate. Several controls were performed to evaluate the possibility that the transients could have originated from the force recording system itself. The stiffness of a fiber of known elastic properties ("mock rubber cell") was determined with our force transducer from either the slope of the instantaneous $L{:}F$ (see Fig. 8*A*) or from the change in steady state tensions before and after the length step ($E = 0.20 \times 10^4$ mN/mm^2) and these stiffness values agree with those reported in the literature. These data indicate that the transducer system was capable of accurately recording both steady state and rapidly changing forces ($\leq$400 Hz) in the range of interest ($\leq$10 μN). When investigating transients recorded from single SMC, we observed that the form of the transient was highly dependent upon the contractile state of the fiber. Specifically, transients were not observed in the relaxed cell, although upon activation their existence became readily apparent. Second, in both the rigor-like and glutaraldehyde-fixed cells in which force was maintained, the transients lacked the characteristic tension recovery normally observed once peak force was obtained. These results suggest that the transients reflect the mechanical properties of structures that are involved in the active production of force, presumably the cross-bridges. If the elastic response does in fact originate within the cross-bridge, one might expect that as force increases, presumably by the recruitment of cross-bridges in a parallel fashion, fiber stiffness (i.e., the sum of cross-bridge stiffnesses) should increase proportionately.

To investigate the relationship of fiber stiffness to force during the development of force after activation, the speed (<5 ms) and extent of length change (<1% L_{cell}) resulting in a true elastic response were determined. Under these conditions, stiffness was directly related to force during force development in accordance with the hypothesis that the elastic response originates in cross-bridges recruited as force increases. Although a similar proportionality between stiffness and force would be obtained if the elasticity resides in some structures having an exponential

L:F in series with the entire contractile system,[1] we believe this is unlikely. If an exponential series elasticity did exist, then the L:F for a 0.5% release in length at various force levels during development of force upon activation should superimpose upon an L:F for a 5% release at the peak of contraction. The point is that a true series elasticity would possess an L:F at any force level during force development that should superimpose upon a segment of its L:F obtained at the peak of contraction that extends over a wider range of forces as a result of the much longer release. Notice in Fig. 19 that the L:F do not always superimpose. Especially at the onset of force development, the L:F have a much steeper slope when compared with a similar section of L:F obtained at the peak of contraction. Therefore, we believe that the existence of a series exponential elasticity is unlikely and that the transients originate in cross-bridges that have a linear elasticity as in striated muscle. As for the nonlinear appearance of the L:F, the existing data indicate that this nonlinearity is due to rapid recovery processes that occur during the step since the nonlinearity is highly dependent upon the time for completion of the step (see Fig. 17). We have recently reported (Warshaw and Fay, 1983*b*) that by assuming the existence of such a rapid recovery superimposed upon the true elastic response, the underlying elasticity would be predicted to possess linear characteristics as in striated muscle.

Cross-Bridge Elasticity

As indicated above, the elasticity in SMC appears to be linear as in striated muscle. This elasticity is linear over a much wider range of length steps than reported by Pfitzer et al. (1982) for hog carotid arteries and is strikingly different from the exponential elasticity reported in other smooth muscle tissue studies (Halpern et al., 1978; Hellstrand and Johansson, 1979; Mulvany, 1979). Although the exponential elasticity in these tissue studies may in part reflect the superposition of a tension recovery during the step upon the elastic response of the cells, it probably also represents the elastic response of the connective tissue matrix. Evidence for a significant extracellular elasticity in tissue was confirmed by high time resolution photographs of SMC within the media of small mesenteric arteries, where it was shown that at least 20% of the tissue elasticity was external to the cell (Mulvany and Warshaw, 1981). In

[1] The proportionality between stiffness and force could be obtained if a true series elasticity existed having an exponential length:force characteristic. The following mathematical treatment illustrates this point:

exponential length:force characteristic for series elasticity: $F = Ae^{Bl}$; (1)

stiffness by definition: $dF/dl = BAe^{Bl}$; (2)

substituting Eq. 1 into 2: $dF/dl = BF$.

Therefore, stiffness would be proportional to force.

addition, Dobrin and Canfield (1977), using proteolytic enzymes against connective tissue proteins, concluded that a significant fraction of the tissue series elasticity in canine carotid arteries must reside within the elastin matrix external to the cells. Therefore, the interpretation of tension transients from tissue studies is complicated by an exponential

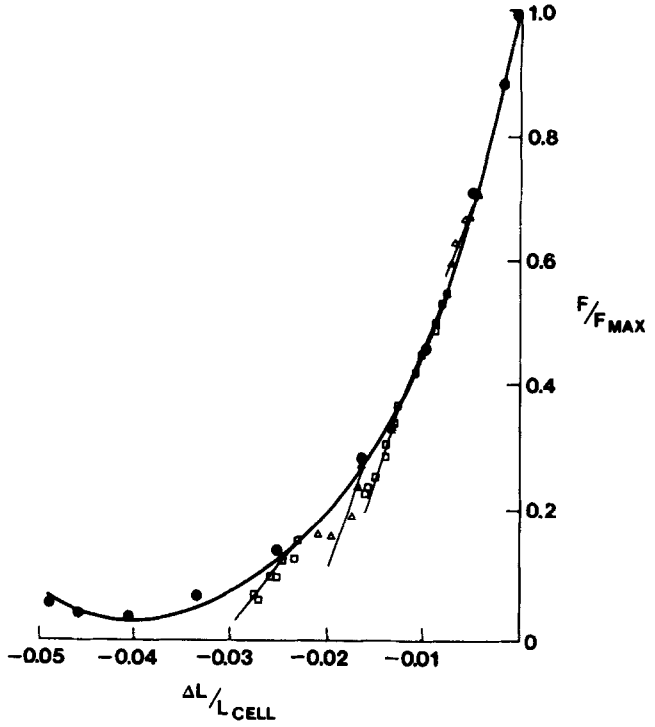

FIGURE 19. Relationship between length and force during a length step applied at various times during active force development. To test whether an exponential series elasticity (see text) is present in single SMC and if its presence can account for the direct relationship between stiffness and force during force development (see Fig. 18), a series of 0.5% L_{cell} releases was imposed at different force levels during development of force upon activation, and then upon reaching the peak of contraction (F_{max}), a large, 5.0% L_{cell} release was applied. If an exponential series elasticity was present, then the L:F for the smaller releases should superimpose upon the segment of L:F from the large release that passes through a similar set of force values. Notice that at force levels between 5 and 40% F_{max} the L:F do not superimpose, which suggests that an exponential series elasticity does not exist. L_{cell} = 134 μm; diam = 3.5 μm; F_{max} = 1.56 μN.

series elasticity through which the cellular responses must be transmitted. Although the single cell's elastic response appears linear as in striated muscle, its compliance (i.e., 1/stiffness) is three times greater than frog fast striated muscle (Ford et al., 1977), in which a 0.5% release will drop force to zero, whereas a 1.5% release is required in SMC (Fig. 20). How

might this increased fiber compliance in SMC be brought about? Since fiber compliance may reflect the manner in which cross-bridges are both arranged as well as the properties of the cross-bridges themselves, we will consider the following possible causes for the increased compliance in SMC: (*a*) existence of a shorter effective sarcomere; (*b*) existence of an undetected series compliance; (*c*) existence of an undetected fast recovery process; (*d*) alterations in cross-bridge population distributions; (*e*) alterations in cross-bridge compliance.

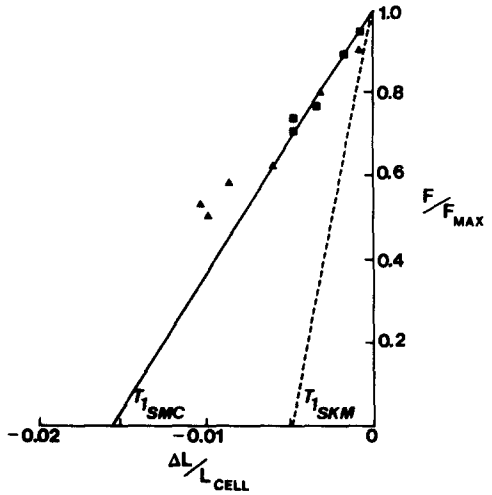

FIGURE 20. Comparison of the relationship between length and force in single smooth and skeletal muscle fibers in response to rapid releases. The L:F shown for an SMC was obtained at the peak of force production (F_{max}) using releases of either 0.5% L_{cell} (■) or 1.0% L_{cell} (▲). Plotted are force (F) during the release (ΔL) vs. length. A linear extrapolation to zero force is shown for the smooth muscle cell ($T1_{smc}$) and that for a fast striated muscle ($T1_{skm}$) from Ford et al. (1977; Fig. 13). Notice that the ΔL to drop force to zero for the SMC is 1.5%, whereas the striated muscle fiber requires only 0.5% ΔL. SMC: L_{cell} = 217 μm; diam = 2.8 μm; F_{max} = 1.25 μN; T = 20°C. SKM: sarcomere length, 2.2 μm; active stress = 290 mN/mm^2; T = 2.5°C.

EXISTENCE OF A SHORTER EFFECTIVE SARCOMERE To compare fiber compliance between SMC and striated muscle at the cross-bridge level, the fiber compliance should be normalized relative to the effective half-sarcomere. If we assume that the high fiber compliance in SMC is due solely to the manner in which myosin is arranged within the cell as opposed to an alteration in the cross-bridge itself, then the effective half-sarcomere in SMC must be 0.3 μm.[2] This value does not agree with

[2] In fast striated muscle, a 0.5% release in muscle length is required to drop maximum isometric force to zero. This length step is equivalent to a 55-Å length change per half-sarcomere (i.e., 1.1 μm). However, in SMC, a 1.6% release is necessary to reduce force to zero. If we assume that in SMC a similar 55-Å release is required to lower force to zero as in striated muscle, then the effective half-sarcomere would be 0.3 μm.

structural data for smooth muscle from either these amphibia or other species. For one, thick filament lengths that have been measured in smooth muscle (Ashton et al., 1975) are longer than in striated muscle, which suggests a longer sarcomere in smooth muscle. In addition, recent immunocytochemical studies in single SMC (Fay et al., 1983) reveal the presence of discretely stained cytoplasmic bodies that demarcate the boundaries of adjacent sarcomere-like units that have a mean length of 2.2 μm in relaxed cells. The discrepancy between the structurally observed value and that calculated from the mechanical experiments suggests that the increased compliance in SMC is not due to the presence of shorter sarcomeres but rather cross-bridges whose apparent mechanical properties are quite different than in striated muscle.

EXISTENCE OF AN UNDETECTED SERIES COMPLIANCE Although the data suggest the presence of a more compliant population of cross-bridges in SMC, several aspects of these measurements must be considered before accepting the possibility of a cross-bridge in SMC having an increased compliance relative to that in fast striated muscle. One possibility as yet unconsidered is that the cross-bridge in SMC is in fact mechanically similar to that in fast striated muscle, but upon its attachment to actin a more compliant structure is recruited in series with each cross-bridge. The increased compliance could reside within the actin filament itself or in actin's attachment to either cytoplasmic or membrane-dense bodies. If, for instance, an SMC cross-bridge can interact with only one actin filament to which no other cross-bridge can attach, then a compliant structure in each filament or in the attachment of the filament to a dense body would be recruited with each individual cross-bridge. Given the known dimensions for a vascular SMC myosin filament of 2.2 μm (Ashton et al., 1975), having a cross-bridge spacing of 144 Å (Lowy et al., 1973), ~76 actin filaments per half-sarcomere per thick filament would be required. Since only 15 actins to 1 myosin has been reported (Ashton et al., 1975), it appears that a series compliance within actin filaments cannot fully account for the apparent increased cross-bridge compliance in SMC.

EXISTENCE OF AN UNDETECTED FAST RECOVERY PROCESS Another possibility for the high compliance in SMC relative to fast striated muscle is that a very rapid recovery occurs during the length step that is of sufficient magnitude and rate, yielding what might appear to be a more compliant cross-bridge in SMC. Presumably this rapid recovery is not detected because of limitations in the time resolution of our present force transducer. Let us briefly pursue this possibility. If we assume that the SMC cross-bridge is no less compliant than in fast striated muscle, we can calculate the extent and rate of recovery required to diminish the elastic response of a fast striated cross-bridge to that observed in our single SMC. To obtain the elastic response, we recorded from an SMC in response to a 0.75% release in length complete in 5 ms; a recovery having a time constant of 0.5 ms capable of 67% recovery would have to be superimposed upon an elastic response of a fast striated muscle cross-bridge. If in

fact this recovery exists in our cells, then a similar rapid recovery must exist during releases of similar amplitude but varying duration (i.e., 1.7 and 25 ms). However, the calculated elastic responses for an SMC, assuming the presence of such an undetected rapid recovery and a striated muscle cross-bridge elastic response, do not match those recorded. For the slower release, the calculated response has an $L{:}F$ significantly less steep than observed, whereas the faster release would have an $L{:}F$ far steeper than observed. This mismatch suggests that the goodness of fit to the 5-ms response was fortuitous and that the presence of such a rapid recovery in our cells is unlikely.

CROSS-BRIDGE PROPERTIES *Theoretical Formalism.* Since it appears unlikely that the high compliance of SMC can be explained by the existence of either a series elasticity of high compliance or an undetected fast recovery during the length step, it becomes more apparent that we must focus our attention on the myosin cross-bridge itself and possible alterations in its structure to account for the observed increased compliance (i.e., decreased stiffness). Although stiffness is a gross mechanical measurement, it is an index of the forces required to make adjustments in the positions of adjacent molecules that make up the structure being tested. In thermodynamic terms, molecules prior to any positional adjustments will exist at a particular free-energy level. Once shifted in position, they will then assume a new free-energy level that will either have required energy to attain this new spatial arrangement or will have liberated energy that can be used to perform work. These simple thermodynamic considerations underly T. L. Hill's (1974, 1975) formalism of muscle contraction.

Although several elegant models for muscle contraction exist and have helped us conceptualize the molecular events that result in force generation (Huxley and Simmons, 1971; Podolsky and Nolan, 1972; Julian et al., 1974), we chose to interpret our data using the Hill (1974, 1975) formalism, as it encompasses many of the concepts addressed in these other models. Because of the general nature of its thermodynamic premise, there is no need to postulate the location of the elasticity or the configurational change within the cross-bridge during force production. In applying this model, we need only specify the distribution of attached cross-bridge states in SMC as well as the mechanical properties of the cross-bridge. The available biochemical data for smooth muscle support the existence of an actomyosin ATPase cycle that has intermediate steps identical to those in striated muscle (Marston and Taylor, 1980). We will therefore assume that, as in fast striated muscle, a distribution of two attached cross-bridge states exists in SMC that is characterized as either a low or high force-producing state (see Fig. 21*A*). Since force is related to the change in free energy per unit axial displacement of the cross-bridge head relative to its actin binding site (i.e., slope of free-energy profile), the low- and high-force states are described by their range of attachments and their corresponding free energies. We will begin by assuming that

the free-energy profiles for both states in SMC are parabolic and identical to those in fast striated muscle. This is equivalent to assuming that each SMC cross-bridge possesses a linear elasticity[3] that is as stiff as in fast striated muscle.

Alterations in Cross-Bridge Population Distribution. Given this formulation, the increased length change required to drop force to zero observed in SMC can be explained at least in part by an alteration in the relative percentages of the attached cross-bridge population that exist in the low and high force-producing states as compared with striated muscle. Let us

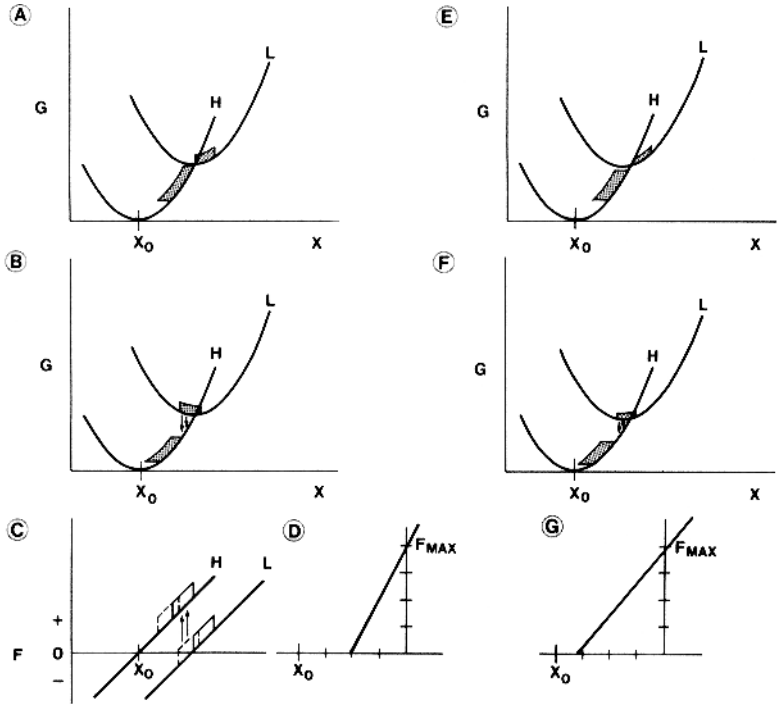

[3] The parabolic free-energy profile defines a cross-bridge elasticity that is linear as determined in the following equations (also see Hill, 1974):

$$\text{Free energy } (G) = A_i + BX^2, \text{ (1)}$$

where A_i equals minimum free energy for a particular cross-bridge state, X equals the axial displacement of cross-bridge head relative to its actin binding site, and B equals a constant.

$$\text{Force } (F) = dG/dX = 2BX; \text{ (2)}$$

$$\text{stiffness } (K) = dF/dX; \text{ (3)}$$

$$\text{substituting Eq. 2 into 3, } K = 2B. \text{ (4)}$$

Therefore, a parabolic free-energy profile defines a linear cross-bridge elasticity.

FIGURE 21. (*opposite*) Theoretical free-energy profiles for cross-bridges in smooth and skeletal muscle. (*A*) The relationship between cross-bridge free energy (*G*) and the axial displacement (*X*) of the cross-bridge relative to its actin binding site for two populations of attached cross-bridges (H and L) in a skeletal muscle fiber according to Hill (1974, 1975). It is assumed that both H and L bridges possess parabolic *G* profiles in accord with their linear elastic properties.[5] Since the slope of *G* defines the force being generated by a cross-bridge at any *X*, the range of attachment for the two populations (shaded regions) dictates that one population be in a low force-producing state (L) near their minimum *G*, whereas the second population exists in a high force-producing state (H) (see Fig. 21*C*). Although the shaded regions illustrate the relative population distribution of cross-bridges between the two states, they do not represent the actual distribution, which is believed to be Gaussian about the minimum *G* for the L state at peak steady state force. (*B*) A rapid release in cell length is illustrated. The H bridges are shifted to lower force values, whereas the L bridges move into a negative force region (see *D*). Immediately after the release, L bridges, being at higher *G*'s relative to *G*'s for H bridges at the same *X*, will make a rapid transition from the L to H state (arrows) and this transition is believed to result in the rapid recovery of force observed immediately after the release. (*C*) The relationships between force (*F*) and cross-bridge position are plotted for both H and L cross-bridges. The solid-lined boxes represent the population distribution for the two cross-bridge states at steady state before the release. The dashed-lined boxes indicate their new position immediately after the release. Notice that both H and L bridges are shifted to lower force values with some L bridges expected to produce negative force. Arrows represent those L bridges that rapidly make the transition to the higher force state upon completion of the step, as indicated in *B*. (*D*) The resulting length:force relationship for a fiber given an equal distribution of cross-bridges in the H and L states is shown. Notice that the release required to drop force to zero is much less than would be necessary (X_o) if all bridges were in the H state. X_o is the minimum *G* for which H bridge force equals zero. A smaller release is required to drop force to zero since a significant fraction of cross-bridges exist in the L state and when shifted upon release contribute negative forces, thus dropping fiber force much more steeply, as opposed to only H bridges being shifted along their *G* profiles. (*E*) A proposal to explain the increased length change required to drop force to zero in SMC based upon an uneven distribution of H and L bridges during steady state contraction. Illustrated schematically is an 80:20 distribution of H vs. L bridges for cross-bridges having similar *G* profiles as in a skeletal muscle fiber (see *A*). (*F*) A release of equal magnitude is imposed as in *B* with both H and L bridges shifted along their *G* profiles. One consequence of the unequal distribution of H and L bridges is that upon completion of the step, fewer cross-bridge are available for the transition between L and H; therefore, the rapid recovery of force would not be as extensive as in *B*. (*G*) The resultant normalized length:force relationship for the unequal distribution of H and L bridges indicates that a greater release is required to drop force to zero, as compared with *D*. The greater release is due to fewer L cross-bridges being shifted into the negative force region during the step.

illustrate this point with an example. A rapid release will result in a shift along their free-energy profiles as shown in Fig. 21*B* and *C* for both low- and high-force attached cross-bridges. The release in length will drop the high-force bridges to a lower free-energy level, thereby reducing the force on these cross-bridges, and the population of attached low force-producing cross-bridges, being near the minimum free energy, is then drawn into a negative force-producing state (see Fig. 21*B* and *C*). The greater the number of cross-bridges in this negative force region, the smaller the fiber force will be at the end of a given length step, resulting in a steeper normalized *L*:*F* (Fig. 21*D*). It is possible that in SMC relatively fewer cross-bridges are attached in the low-force state (Fig. 21*E* and *F*), thereby decreasing the negative force contribution and thus increasing the length changed required to drop force to zero (Fig. 21*G*). This shift in the low/high ratio compared with striated muscle may in part account for the greater percent length change needed to drop force to zero. Such a change in the ratio of low to high force generators would be expected to alter the extent of recovery of tension after the step is complete. Briefly, since the rapid tension recovery after completion of the step is believed to reflect the transition of the low-force cross-bridges in the negative-force region to the high-force state (Fig. 21*B* and *C*), then fewer low-force cross-bridges would be available for this transition, resulting in a less extensive fast phase of tension recovery in SMC as compared with striated muscle. This prediction is in fact substantiated by data in single SMC (Warshaw and Fay, 1983*b*).

Alteration in Cross-Bridge Compliance. Although a difference in the population distribution of cross-bridges in SMC may exist, it cannot account fully for the longer release necessary to drop force to zero that was observed in our SMC as compared with fast striated muscle. Therefore, we must consider that the cross-bridge in SMC is also significantly different than in fast striated muscle, being inherently more compliant. What effect a more compliant cross-bridge may have on SMC's contractile characteristics can best be addressed by returning to the cross-bridge free-energy profiles.

If we assume that the SMC cross-bridge is inherently more compliant, then the free-energy profiles must be altered in the manner shown in Fig. 22*A*. The shape of the free-energy profile remains parabolic because the cross-bridge elasticity remains linear in SMC. However, the curvature must be decreased to account for the increased compliance. These changes in the shape of the profiles have some important consequences for the contractile properties of SMC as we will now discuss.

Since ATP is the energy source for contraction in SMC as in fast striated muscle, the maximum energy available to perform work should be identical for the two muscle types. If the maximal cross-bridge free energies are equal for smooth and fast striated muscle, then the slope of the free-energy profile at this maximum free-energy level will be less in smooth than in fast striated muscle (see Fig. 22*A*). As the slope of this

free-energy curve is equivalent to force, the decreased slope at the cross-bridge maximum free energy indicates that the maximum force per cross-bridge is reduced in SMC. However, the force per muscle cross-sectional area generated by our SMC is equivalent to that in striated muscle. If in fact the force per cross-bridge is reduced in SMC, then in order to reconcile the apparent discrepancy, an offsetting increase in the percentage of the cross-bridge cycle time spent in the attached high force-

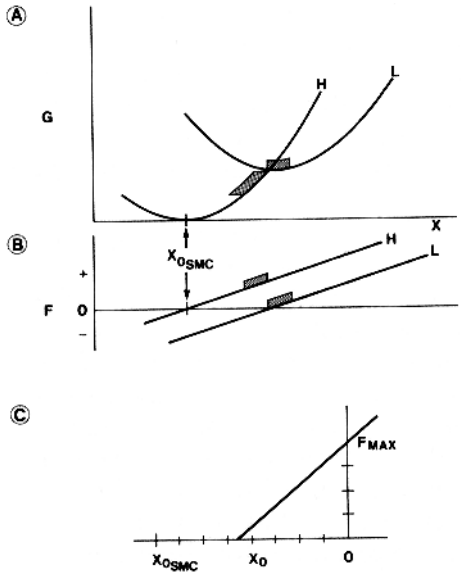

FIGURE 22. Theoretical free-energy curves for cross-bridges in smooth muscle, indicating an additional cause for increased compliance. (*A*) Free-energy profiles in a SMC for two populations of cross-bridges being inherently more compliant relative to skeletal muscle. Since the cross-bridges are assumed to possess linear elastic properties, the high- (H) and low- (L) force cross-bridge free-energy (*G*) profiles remain parabolic but are less curved than in Fig. 21*A* and *E*. It is assumed that an equal distribution of cross-bridges exists in both the H and L states. (*B*) The relationship of force (*F*) vs. cross-bridge position (*X*) for both H and L states is shown. Notice that the forces are much lower than in Fig. 21*B* as predicted by the less curved *G* profiles. (*C*) The *L*:*F* for a cell containing cross-bridges with increased compliance, as in *A*.

producing state relative to fast striated muscle must be postulated for SMC. Support for this prediction can be found in biochemical studies of the interaction between actin and myosin in smooth muscle. Krisanda and Murphy (1980) have reported that once smooth muscle myosin attaches to skeletal muscle actin, it will remain attached much longer than would striated muscle myosin; similar conclusions are reached upon consideration of the magnitude and time course of recovery during tension transients in single smooth muscle cells (Warshaw and Fay, 1983*a*). Further

support for the notion that cross-bridge lifetime is increased in SMC comes from considering what effect an increased cross-bridge compliance may have on cross-bridge kinetics. Since a myosin cross-bridge will only attach to an actin binding site that is within a range of positions favorable for attachment, the increased flexibility or working range could allow a given cross-bridge to interact with many more actin binding sites. Therefore, a greater percentage of cross-bridges may encounter a favorable actin site and thereby generate force. Support for the hypothesis that SMC cross-bridge flexibility is increased relative to striated muscle comes from both hydrodynamic and electron microscopic data that have recently been reported to indicate an increased flexibility of the SMC myosin monomer (Onishi and Wakabayashi, 1982; Trybus et al., 1982). The exact location of this flexibility has not yet been determined, but its existence appears to support our contention that the cross-bridge in SMC is more compliant.

Similarities with Slow Striated Muscle. Although the cross-bridge compliance in SMC appears to be much greater than in fast striated muscle, comparison of SMC's cross-bridge properties with those of slow striated muscle may be more reasonable since the two muscle types exhibit a slow, economical contraction. Heinl et al. (1974), studying tension transients in tortoise striated muscle, have presented data suggesting that the cross-bridge in this muscle is also more compliant than in fast striated muscle. In fact, the cross-bridge compliance in tortoise striated muscle is considerably greater than in fast striated muscle. The fact that tortoise striated muscle is similar in structure to fast striated muscle argues against structural differences as an explanation for the increased compliance between these fiber types. The question then arises as to how the alteration in cross-bridge compliance for both the tortoise striated muscle and SMC is linked to the significant differences in their contractile properties as compared with fast striated muscle. Although at present the answer is not immediately obvious, it appears that a compliant cross-bridge may in some way be necessary for the expression of the unique physiological characteristics observed in slow economical muscles.

Summary

The results of this study indicate that transients obtained in single SMC are a true reflection of the structures involved in force generation, the cross-bridge. Although the SMC cross-bridge elasticity appears linear as in striated muscle, cross-bridge stiffness and the percentage of cross-bridges in the low-force state may be much smaller in smooth muscle. Some insight as to how the decreased cross-bridge stiffness in SMC is brought about was obtained by assuming a thermodynamic model similar to that previously described in striated muscle. As a consequence of the greater cross-bridge working range, force per cross-bridge is reduced and therefore a cross-bridge must spend a greater percentage of the total cycle time in a high-force state to account for SMC's capability of produc-

ing forces per square millimeter comparable to those in striated muscle. The increased flexibility may allow more of the SMC cross-bridges to interact with actin binding sites, thus increasing the probability of attachment and force generation. Since the overall time course for the tension transients is longer in SMC, which suggests a longer cross-bridge cycle time, less ATP would be required to maintain force in SMC. Therefore, smooth muscle's unique physiological contractile properties of a high ATP economy for maintaining force (Paul et al., 1976; Siegman et al., 1980), as well as a slower velocity of contraction, may be a reflection of a slight change in the structure of the myosin molecule, which may have profound effects upon the mechanical behavior of the cross-bridge and the kinetics of its cycle.

We would like to thank Ms. R. Hoffman, S. LeClair, and M. Small for their technical assistance, Mr. K. Fogarty for his development of the computer programs, Mr. C. Rodgers for his fine machining skills, Ms. P. McNamee for her artistic talent in figure illustrating, and Ms. S. Reed for her patience in typing the numerous versions of this manuscript.
During the period of this study, D. M. Warshaw was supported by postdoctoral fellowships from the National Institute of Health (HL 05770) and the Muscular Dystrophy Association, and F. S. Fay was supported by grants from the National Institutes of Health (HL 14523) and the Muscular Dystrophy Association.

Received for publication 31 January 1983 and in revised form 29 March 1983.

REFERENCES

Alexander, R. S. 1976. Series elasticity of urinary bladder smooth muscle. *Am. J. Physiol.* 231:1337–1343.

Ashton, F. T., A. V. Somlyo, and A. P. Somlyo. 1975. The contractile apparatus of vascular smooth muscle: intermediate high voltage stereo electron microscopy. *J. Mol. Biol.* 98:17–29.

Canaday, P. G., and F. S. Fay. 1976. An ultrasensitive isometric force transducer for single smooth muscle cell mechanics. *J. Appl. Physiol.* 40:243–246.

Cohen, D. M., and R. A. Murphy. 1979. Cellular thin filament protein contents and force generation in porcine arteries and veins. *Circ. Res.* 45:661–665.

Cox, R. H. 1977. Determination of the series elasticity in arterial smooth muscle. *Am. J. Physiol.* 233:H248–H255.

Dobrin, P., and T. Canfield. 1977. Identification of smooth muscle elastic component in intact carotid artery. *Am. J. Physiol.* 232:H122–H130.

Fay, F. S., P. H. Cooke, and P. G. Canaday. 1976. Contractile properties of isolated smooth muscle cells. *In* Physiology of Smooth Muscles. E. Bulbring and M. F. Shuba, editors. Raven Press, New York. 249–264.

Fay, F. S., K. Fujiwara, D. D. Rees, and K. E. Fogarty. 1983. Distribution of α-actinin in single isolated smooth muscle cells. *J. Cell Biol.* 96:783–795.

Fay, F. S., R. Hoffman, S. Leclair, and P. Merriam. 1982. Preparation of individual smooth muscle cells from the stomach of *Bufo marinus*. *Methods Enzymol.* 85:284–292.

Fay, F. S., D. D. Rees, and D. M. Warshaw. 1981. The contractile mechanism in smooth muscle. *In* Membrane Structure and Function. E. E. Bittar, editor. John Wiley & Sons, New York. 4:79–130.

Fay, F. S., and J. J. Singer. 1977. Characteristics of response of isolated smooth muscle cells to cholinergic drugs. *Am. J. Physiol.* 232(3):C144–C154.

Fenn, W. O. 1923. A quantitative comparison between the energy liberated and the work performed by the isolated sartorius of the frog. *J. Physiol. (Lond.).* 58:175–203.

Ford, L. E., A. F. Huxley, and R. M. Simmons. 1977. Tension response to sudden length change in stimulated frog muscle fibers near slack length. *J. Physiol. (Lond.).* 269:441–515.

Guth, K., H. J. Kuhn, B. Drexler, W. Berberich, and J. C. Ruegg. 1979. Stiffness and tension during and after sudden length changes of glycerinated single insect fibrillar muscle fibers. *Biophys. Struct. Mechanism.* 5:255–276.

Halpern, H., M. J. Mulvany, and D. M. Warshaw. 1978. Mechanical properties of smooth muscle cells in the walls of arterial resistance vessels. *J. Physiol. (Lond.).* 275:85–101.

Heinl, P., H. J. Kuhn, and J. C. Ruegg. 1974. Tension responses to quick length changes of glycerinated skeletal fibers from the frog and tortoise. *J. Physiol. (Lond.).* 237:243–258.

Hellstrand, P., and B. Johansson. 1979. Analysis of the length response to a force step in smooth muscle from rabbit urinary bladder. *Acta Physiol. Scand.* 106:231–238.

Hill, T. L. 1974. Theoretical formalism for the sliding filament model of contraction of striated muscle. Part I. *Prog. Biophys. Mol. Biol.* 28:267–340.

Hill, T. L. 1975. Theoretical formalism for the sliding filament model of contraction of striated muscle. Part II. *Prog. Biophys. Mol. Biol.* 29:105–159.

Huxley, A. F., and R. M. Simmons. 1971. Proposed mechanism for force generation in striated muscle. *Nature (Lond.).* 233:533–538.

Julian, F. J., and M. R. Sollins. 1975. Variation of muscle stiffness with force at increasing speeds of shortening. *J. Gen. Physiol.* 66:287–302.

Julian, F. J., K. R. Sollins, and M. R. Sollins. 1974. A model for the transient and steady-state mechanical behavior of contracting muscle. *Biophys. J.* 14:546–562.

Kawai, M., P. W. Brandt, and M. Orentlicher. 1977. Dependence of energy transduction in intact skeletal muscles on the time in tension. *Biophys. J.* 18:161–172.

Krisanda, J. M., and R. A. Murphy. 1980. Tight binding of arterial myosin to skeletal F-actin. *J. Biol. Chem.* 255:10771–10776.

Lowy, J., P. J. Vibert, J. C. Haselgrove, and F. R. Poulsen. 1973. The structure of myosin elements in vertebrate smooth muscles. *Phil. Trans. R. Soc. Lond. B Biol. Sci.* 265:191–196.

Marston, S. B., and E. W. Taylor. 1980. Comparison of the myosin and actomyosim ATPase mechanisms of the four types of vertebrate muscles. *J. Mol. Biol.* 139:573–600.

McLaughlin, R. J. 1977. Systematic design of cantilever beams for muscle research. *J. Appl. Physiol.* 42:786–794.

Meiss, R. A. 1978. Dynamic stiffness of rabbit mesotubarium smooth muscle: effect of isometric length. *Am. J. Physiol.* 234:C14–C26.

Mulvany, M. J. 1979. The undamped and damped series elastic components of a vascular smooth muscle. *Biophys. J.* 26:401–414.

Mulvany, M. J., and D. M. Warshaw. 1981. The anatomical location of the series elastic component in rat vascular smooth muscle. *J. Physiol. (Lond.).* 314:321–330.

Murphy, R. A. 1976. Contractile system function in mammalian smooth muscle. *Blood Vessels.* 13:1–23.

Onishi, H., and T. Wakabayashi. 1982. Electron microscopic studies of myosin molecules

from chicken gizzard muscle. I. The formation of the intramolecular loop in the myosin tail. *J. Biochem. (Tokyo).* 92:871–880.

Paul, R. J., E. Gluck, and J. C. Ruegg. 1976. Cross-bridge ATP utilization in arterial smooth muscle. *Pflügers Arch. Eur. J. Physiol.* 361:297–299.

Pfitzer, G., J. W. Peterson, and J. C. Ruegg. 1982. Length dependence of calcium activated isometric force and immediate stiffness in living and glycerol extracted vascular smooth muscle. *Pflügers Arch. Eur. J. Physiol.* 394:174–181.

Podolsky, R. J., and A. C. Nolan. 1972. Muscle contraction transients, cross-bridge kinetics, and the Fenn effect. *Cold Spring Harbor Symp. Quant. Biol.* 37:661–668.

The Sea Scout Manual. 1939. Boy Scouts of America, New York. 303.

Siegman, M. J., T. M. Butler, S. V. Mooers, and R. E. Davies. 1980. Chemical energetics of force development, force maintenance, and relaxation in mammalian smooth muscle. *J. Gen. Physiol.* 76:609–629.

Trybus, K. M., T. W. Huiatt, and S. Lowey. 1982. A bent monometric conformation of myosin from smooth muscle. *Proc. Natl. Acad. Sci. USA.* 79:6151–6155.

Warshaw, D. M., and F. S. Fay. 1983*a*. Do smooth muscle's contractile capabilities reflect unique cross-bridge properties? *Biophys. J.* 41:153*a*. (Abstr.)

Warshaw, D. M., and F. S. Fay. 1983*b*. Tension transients in single isolated smooth muscle cells. *Science (Wash. DC).* 219:1438–1441.

Warshaw, D. M., M. J. Mulvany, and W. Halpern. 1979. Mechanical and morphological properties of arterial resistance vessels in young and old spontaneously hypertensive rats. *Circ. Res.* 45:250–259.